Plant flavones enrich rhizosphere *Oxalobacteraceae* to improve maize performance under nitrogen deprivation

Peng Yu[1,2,3,#], Xiaoming He[1,2,3,#], Marcel Baer[2], Stien Beirinckx[4,5,6], Tian Tian[7], Yudelsy A.T. Moya[8], Xuechen Zhang[9], Marion Deichmann[10], Felix P. Frey[2], Verena Bresgen[2,3], Chunjian Li[11], Bahar S. Razavi[12], Gabriel Schaaf[10], Nicolaus von Wirén[8], Zhen Su[7], Marcel Bucher[13,14], Kenichi Tsuda[15,16], Sofie Goormachtig[4,6], Xinping Chen[1,*], Frank Hochholdinger[1,2,*]

[1] College of Resources and Environment, and Academy of Agricultural Sciences, Southwest University (SWU), Chongqing 400715, China

[2] Crop Functional Genomics, Institute of Crop Science and Resource Conservation (INRES), University of Bonn, Bonn 53113, Germany

[3] Emmy Noether Group Root Functional Biology, Institute of Crop Science and Resource Conservation (INRES), University of Bonn, Bonn 53113, Germany

[4] Department of Plant Biotechnology and Bioinformatics, Ghent University, 9052 Gent, Belgium

[5] Plant Sciences Unit, Flanders Research Institute for Agriculture, Fisheries and Food (ILVO), 9820 Merelbeke, Belgium

[6] Center for Plant Systems Biology, VIB, 9052 Ghent, Belgium

[7] State Key Laboratory of Plant Physiology and Biochemistry, College of Biological Sciences, China Agricultural University, Beijing 100193, China

[8] Molecular Plant Nutrition, Leibniz Institute of Plant Genetics and Crop Plant Research (IPK), Gatersleben 06466, Germany

[9] Department of Biogeochemistry of Agroecosystems, University of Göttingen, Göttingen 37077, Germany

[10] Plant Nutrition, Institute of Crop Science and Resource Conservation (INRES), University of Bonn, Bonn 53113, Germany

[11] Department of Plant Nutrition, College of Resources and Environmental Science, China Agricultural University, Beijing 100193, China

[12] Department of Soil and Plant Microbiome, Institute of Phytopathology, Christian-Albrecht-University of Kiel, Kiel 24118, Germany.

[13] Botanical Institute, Cologne Biocenter, University of Cologne, Cologne 50674, Germany

[14] Cluster of Excellence on Plant Sciences (CEPLAS), University of Cologne, 50674 Cologne, Germany

[15] State Key Laboratory of Agricultural Microbiology, College of Plant Science and Technology, Huazhong Agricultural University, Wuhan 430070, China

[16] Department of Plant Microbe Interactions, Max Planck Institute for Plant Breeding Research, Cologne 50829, Germany

Introduction

During domestication and improvement of plants from natural ecosystems to modern agriculture, root systems rapidly extended their functionality and complexity[1,2]. Root-mediated processes are responsible for major changes in physical and chemical properties of the rhizosphere, which defines the soil volume that is influenced by the properties of the root[3]. It represents a unique soil environment in which complex biogeochemical processes and dynamic biological interactions occur that are mainly driven by plant roots via their secretory activities and soil microorganisms designated the rhizosphere microbiota[4]. Plant-soil-microbe interactions in return affect plant growth, development and health[5-8]. An increasing body of evidence highlights the strong influences of edaphic factors and plant genotype on the assembly and function of the rhizosphere microbiota under controlled conditions[9-12]. Plants are able to shape their rhizosphere microbiota, as supported by the observation that different plant species host specific microbial communities when grown in the same soil[13-15]. Plant root systems display extreme developmental plasticity, enabling them to respond to a wide range of environmental conditions[16]. With respect to the microbiome, plant growth-promoting rhizobacteria affect root growth and development by modulating cell division and differentiation[17], leading to changes in root system architecture[18]. However, to date, an association between root architectural traits during development and the composition or diversity of defined microbial taxa has not been established yet in crop species.

Maize (*Zea mays* L.) displays a complex root system architecture[19] and exhibits an exceptional degree of genomic diversity[20]. Hence, maize is an excellent model to explore the relationship between root structure, genetic variation, gene regulation and their interaction with the rhizosphere microbiota. The maize root system comprises different root types that are formed and function at different stages of development[19,21]. Distinct maize root types display specific anatomical characteristics, disparate transcriptomic signatures[22] and divergent responses to nutrient availability[23,24]. The great architectural and functional diversity of the maize root system has the potential to shape the rhizosphere microbiota composition[25]. Specifically, root type-specific metabolic properties influence microbial communities inhabiting respective root types in maize and rice[26-28]. Conversely, it has been suggested that root-associated bacteria contribute to differential nitrogen use efficiencies observed in *indica* and *japonica* rice varieties[29], suggesting that root microbiota could alleviate overall nutrient stress in crops. Different maize genotypes display variation in their bacterial microbiome and specific enrichment of different bacterial taxa[30,31]. Among the different maize germplasm groups, sweet corn displays a unique root exudate composition and a tendency to enrich for bacterial taxa that have been associated with nitrogen-fixing activities in the rhizosphere[31]. Maize root exudates contain a variety of metabolites, including substantial amounts of benzoxazinoids and flavonoids that are secreted into the rhizosphere[32]. Benzoxazinoids released by maize roots drive plant performance and defence by shaping rhizosphere microbiota[33,34]. Flavonoids have been considered crucial root-released rhizosphere signal molecules modulating the interaction of roots with microbes[35,36]. Genes such as *flavone synthase* (*FNS*) and *chalcone synthase colorless2* (*C2*) are critical for flavonoid biosynthesis in maize[37-39]. Root flavonoids are essential for initiating symbiosis with rhizobia in legumes and also act as auxin transport regulators[40,41]. This implies that flavonoid-mediated root-microbe interactions might modulate

developmental processes also in the host plant[36]. Thus, metabolic profiles of specific root types, together with the composition and diversity of microbial taxa in the maize rhizosphere, might be candidate target traits for genetic improvement of nutrient uptake and crop performance under field conditions.

Plants strengthen their association with microbes to optimize nutrient acquisition through developmental adaptations of the root system in nutrient poor soil[42]. Nevertheless, the interplay between plants and microbes at the root-soil boundary and its impacts on microbial communities in the rhizosphere and on plant nutrient acquisition have received little attention so far. Therefore, in the present study we elucidated causal interactions between the rhizosphere microbiota, host genetic variation, and host gene expression influencing root developmental processes and nutrient capture under nitrogen deprivation.

Results

Developmental gradients along the longitudinal root axis differ in their transcriptomic landscape

We subjected three longitudinal zones (Fig. 1a) of second whorl crown roots (Supplementary Fig. 1a) of a diverse panel of 20 field-grown maize inbred lines (Supplementary Fig. 1b) in three biological replicates to a transcriptomics experiment and the attached rhizosphere to a fungal and bacterial microbiome analysis. The three root zones include the meristematic zone and the apical part of the elongation zone (zone 1), the basal part of the elongation zone and the apical part of the differentiation zone with root hairs and emerging lateral root primordia (zone 2) and the basal part of differentiation zone with root hairs and emerged lateral roots (zone 3) (Fig. 1a). The separated longitudinal root zones reflect dynamic patterns of root exudation and nutrient uptake capacity, nutrient availability and microbial density along the rhizosphere[3] (Fig. 1a). A principal component analysis (PCA) together with differential gene analysis illustrated a high transcriptomic similarity between zone 2 and zone 3 in comparison to zone 1 (Fig. 1b; Supplementary Fig. 1c). To confirm functional variation among these zones, differentially expressed genes (Supplementary Dataset 1) were functionally classified by Gene Ontology (GO) term enrichment analyses. In the three pairwise comparisons, genes were specifically enriched for root hair elongation (GO:0048767, FDR <0.01) for zone 1 vs zone 2 and zone 1 vs zone 3 and lateral root development (GO:0048527, FDR <0.05) for zone 2 vs zone 3 and zone 1 vs zone 3 (Supplementary Fig. 1c), highlighting that tissue-specific transcriptome changes are in line with the developmental changes of these traits in the three zones.

We further subjected the root transcriptome data to weighted gene co-expression network analyses (WGCNA) (Supplementary Dataset 2) that cluster genes into modules based on their expression profiles and identified 49 co-expression modules, which are groups of highly interconnected genes exhibiting similar gene expression patterns (Supplementary Dataset 3). Specifically, we detected nine modules (M22-M30) displaying specific enrichment along the root development and six co-expression modules (M22-M27) were gradually depleted during root differentiation from the younger meristematic to the older differentiation zone, while three modules (M28-M30) were enriched in zone 3 for all maize genotypes (Supplementary Fig. 2a). Functional annotation of these modules demonstrated enrichment of specific biological processes along the developmental zones (Supplementary Fig. 2b; Supplementary Dataset 4). Among those, growth module 26 is antagonistically associated with defence module 30 (Fig. 1c), highlighting a balancing growth-defence tradeoff during root differentiation. In particular, the auxin signal transduction and the phenylpropanoid biosynthesis pathways were highly interacting within growth module 26 (Supplementary Fig. 3a; Supplementary Dataset 5). For the defence module 30, the maize hub gene *ACC1* (*acetyl-coenzyme A carboxylase1*, Zm00001d004125) was identified as a central player interacting with pathways associated with secondary metabolism and microbial carbon and nitrogen metabolism (Supplementary Fig. 3b; Supplementary Dataset 6). The production of malonyl-CoA through carboxylation of acetyl-CoA by ACC is postulated to be one of the essential substrates for biosynthesis of fatty acids and flavonoids. Moreover, the interconnecting maize genes *fab1* (*fatty acid biosynthesis1*, Zm00001d025201) encoding fatty acid biosynthesis and *WHP1* (*white pollen 1*, Zm00001d007403) encoding a chalcone synthase involved in the pathway of flavonoid

biosynthesis were identified correspondingly. For nitrogen metabolism, the glutamine synthetase *GLN6* (Zm00001d028260) and the asparagine synthetases *asn3* (Zm00001d028750) and *asn4* (Zm00001d047736) were associated with the flow of ammonium into organic nitrogen compounds (Supplementary Dataset 6). Together, these analyses highlight the enrichment of genes associated with carbon/nitrogen metabolism and potential roles of flavonoids on root-rhizosphere interaction along the crown root of maize.

Bacterial community composition in the rhizosphere shifts along the longitudinal root axis while fungal community composition does not

To understand the microbial taxa distribution in the rhizosphere along the root, we analyzed the bacterial and fungal microbiomes by 16S rRNA and ITS sequencing (see Methods). Rarefaction analysis demonstrated that sequencing of the microbiome had enough coverage to capture most rhizosphere microbial taxa members for each zone of the 20 maize genotypes (Supplementary Fig. 4a). A PCA showed that, regardless of genotype, a strong shift in bacterial community composition is observed in the maize rhizosphere along the developmental zones (Fig. 1d), but not in fungal microbiome composition (Fig. 1e; Supplementary Table 1). Microbiome richness varied between developmental zones. Zone 3 displayed lower bacterial community diversity than zones 1 and 2, while no significant differences were observed between these zones for fungal community diversity (Supplementary Fig. 4b). Substantial differences in the bacterial community structure of bulk and rhizosphere soils were detected (Supplementary Fig. 5a). Seven of the highly abundant phyla (>96%) (Supplementary Fig. 4c) significantly differed between bulk and rhizosphere soil (FDR <0.05; Supplementary Fig. 5b). Of the rhizosphere bacterial phyla with >0.1% abundance, *Proteobacteria* and *Verrucomicrobia* were significantly enriched in zone 3, where lateral root primordia are formed and lateral roots emerge (Supplementary Fig. 5b). In contrast, *Acidobacteria*, *Gemmatimonadetes*, *Chloroflexi* and *Nitrospirae* were depleted from zones 1 to 3 (Supplementary Fig. 5b). Moreover, *Actinobacteria* were always present in the rhizosphere of all three root zones (Supplementary Fig. 5b). To investigate root genotype- or/and zone-dependent rhizosphere microbial OTU (operational taxonomic unit) relationships between bacteria and fungi, a co-abundance network was inferred (Supplementary Dataset 7). Consistent with the PCA data, bacterial OTUs showed complex networks while fungal OTUs did not (Supplementary Fig. 6a). Bacterial OTUs related to *Nitrospirales* showed strong negative correlation with the OTUs corresponding to *Verrucomicrobiales* (Supplementary Fig. 6b). Furthermore, bacterial OTUs related to *Sphingomonadales* and *Verrucomicrobiales* displayed the highest accumulative intra-taxa correlations, although *Burkholderiales* is the main bacterial taxon interacting between the taxa *Sphingomonadales* and *Verrucomicrobiales* (Supplementary Fig. 6c). Thus we hypothesize that changes in composition and diversity of the rhizosphere bacterial microbiome might be associated with transcriptomic divergence along the developmental zones of the root.

Association of the root transcriptome and rhizosphere microbiome along the longitudinal root zones

To associate gene expression and microbial OTU abundance, we filtered root RNA-seq reads and microbial amplicon reads for significant correlations of the factors root genotype, zone and genotype by zone interaction between the datasets (Supplementary Dataset 8; Supplementary Table 2). Co-variance analysis demonstrated that defined genes expressed in the host roots interact stronger with bacterial OTUs than fungal OTUs (20 times differences, FDR <0.001) in the rhizosphere (Fig. 1f; Supplementary Table 3). To identify how the root zones associate with the rhizosphere microbiota across the genotypes, we correlated eigengenes with the relative abundance of microbial taxa as "trait" and looked for the most significant associations. We searched for significant correlations between these microbial taxa and module eigengene expression values and identified 30 genotype- or zone-specific module-based microbial taxa correlations from phylum to species (Supplementary Dataset 9). We further confirmed that host transcriptome modules had much stronger correlations with bacteria than with fungi at the order level (Fig. 1g; Supplementary Dataset 9). Moreover, growth and defence gene modules had distinct relations with different bacterial orders, e.g. the order *Nitrospirales* was most positively related to the growth-related modules (Module 22, 25 and 26) and *Verrucomicrobiales* was negatively related to the defence-related modules (Modules 28-30) (Fig. 1g; Supplementary Dataset 9). Notably, by correlation-based network analyses we demonstrated that root zone-specific gene module expression is strongly associated with specific rhizosphere bacterial taxa along the longitudinal root axis.

Genotype-dependent changes of the root transcriptome and rhizosphere microbiome are synchronized with plant performance

Next, we asked whether maize growth performance is linked with the genotype-specificity of the interaction of its transcriptomic signature with the rhizosphere microbiome. We investigated 20 phylogenetically distinct genotypes and showed that the genotypes performed differently in the field with respect to biomass production, leaf area, photosynthesis and shoot nitrogen accumulation (Supplementary Fig. 7). Among these genotypes, the inbred line 787 displayed highest leaf area, shoot biomass and nitrogen accumulation in comparison to the other genotypes, while LH93 performed poorly under the same field conditions (Supplementary Fig. 7). By subjecting the root transcriptomes of these genotypes to WGCNA, we identified four modules (M1-M4) associated with the four phylogenetic clades (A-D) and 17 modules corresponding to 17 diverse genotypes (Fig. 2a). However, only few of the genotype-specific modules have significantly enriched GO functions (Fig. 2a), indicating that the genetic dissimilarity is not always linked with functional diversity among genotypes. We therefore hypothesized that genotype-dependent changes in root transcriptomes might underlie the observed variations in rhizosphere microbiome. The maize inbred lines 787, which showed a unique bacterial community along the longitudinal rhizosphere (Supplementary Fig. 8a) and its corresponding transcriptomic module 5, displayed the highest correlation with bacterial taxa at the level of phyla and orders compared with all other maize genotypes (Fig. 2b; Supplementary Fig. 8b, c). Moreover, module 5 had a significantly high correlation with the bacterial orders *Clostridiales*, *Bacteroidales*, *Lactobacillales*, *Burkholderiales*, *Chromatiales*, *Opitutales*, *Rhodobacterales* and *Sphingobacteriales* in comparison with the other genotypes (Supplementary Fig. 9). In addition, inbred line 787 displayed a strong tendency to enrich

those taxa that had been predicted in association with nitrogen metabolism and transformation (e.g., *Lachnospiraceae* and *Nitrosomonadaceae*) (Fig. 2c). Interestingly, *Oxalobacteraceae* are exclusively enriched in the rhizosphere of genotype 787 with the highest correlation with module 5 in comparison to other bacterial families in this study (Fig. 2c; Supplementary Fig. 10). At the genus level, relative abundance of *Massilia* is significantly enriched in the rhizosphere of inbred line 787 in comparison to the other maize genotypes except for B73 and W64A (Supplementary Dataset 10). In particular, enrichment of *Oxalobacteraceae* is strongly correlated with growth-related module 26 and module 27 in comparison to the defence-related modules (M28-M30) (Supplementary Dataset 9). Together, these results suggest that specific bacterial taxa become enriched as a consequence of genotype-specific properties and associate with plant nutrition and growth status.

Flavonoid composition coincides with rhizosphere microbiota composition and maize growth properties

To deepen the understanding of the exceptional performance of inbred line 787, we surveyed the 787 transcriptome for genes with exceptional modular connectivity. Among those, *FNSI2* (Zm00001d027423), encoding a flavone synthase displayed the highest modular connectivity within module 5 (Supplementary Dataset 11). Identification of *FNSI2* together with the enrichment of the flavonoid biosynthesis-related genes *ACC1* and *WHP1* in the zone-specific transcriptome analysis highlights the potential importance of flavonoid metabolism and its interaction with rhizosphere microbiota in maize. In line with this observation classical genetic studies demonstrated that root flavonoids are crucial for legume nodule initiation in soybean[41] and Medicago[40]. In particular, flavones and flavonols play distinct and critical roles in root-microbe interaction during legume-rhizbobium symbiosis[43]. Moreover, the transcriptome data suggested that *FNSI2* is specifically expressed in the root cortex. In contrast its paralogue *FNSI1* (Zm00001d029744) is predominantly expressed in leaves (Supplementary Fig. 11). Flavone synthases are critical enzymes that catalyze the conversion of the flavanones naringenin and eriodictyol into apigenin and luteolin[37]. Specifically, roots of the inbred line 787 contained and exudated significantly more apigenin and luteolin flavones than inbred line LH93, which accumulated less *FNSI2* transcripts (Fig. 2d, e). Furthermore, ^{14}C labelling and imaging experiments (Supplementary Fig. 12a) demonstrated that 787 released significantly higher amounts of root exudates to the rhizosphere than LH93 (Supplementary Fig. 12b and c). We then tested whether the 787-dependent variation in rhizosphere microbiota composition was associated with changes in plant performance and nitrogen use. To this end, sterilization and rhizosphere transplantation trials were performed with the vigorous inbred line 787 and the poorly performing inbred line LH93. The maize inbred line 787 produced more dry shoot biomass than LH93 in nitrogen-poor soil, however growth differences between these two genotypes were not observed when grown in sterilized soil (Fig. 2f). When LH93 was transplanted into soil, in which the inbred line 787 had been grown before (787-grown soil), LH93 significantly increased shoot biomass production. In contrast, the inbred line 787 showed significant growth inhibition when it was transferred to soil, in which the inbred line LH93 was grown before (LH93-grown soil) 18 days after transplantation (DAT) (Fig. 2g). After 28 DAT, shoot biomass of the inbred line 787 in LH93-grown soil and 787-grown soil was not significantly different, whereas LH93

performed significantly better in 787-grown soil than in LH93-grown soil (Fig. 2g). In particular, the total nitrogen and available mineral nitrogen of the soil prior to transplantation have no significant differences between 787-grown and LH93-grown soils (Supplementary Fig. 13). Thus, we hypothesized that the rhizosphere microbiota conditioned by the vigorous genotype 787 is sufficient to trigger growth of the poorly performing genotype LH93. To further explore the role of the 787-dependent rhizosphere microbiota, we carried out a shotgun metagenomic sequencing of the rhizosphere microbiota of 787 and LH93 (Supplementary Fig. 14a). The metagenomics data validated that the host-specific microbiota of the inbred line 787 differed from that of the inbred line LH93 (Supplementary Fig. 14b). We performed a functional annotation by comparison of quality-filtered reads of these metagenomes to annotated reads using the Clusters of Orthologous Groups (COG) databases (see methods). This revealed that a number of biogenesis, transport and metabolism related processes were significantly enriched in the rhizosphere microbiota associated with genotype 787 in comparison to LH93 (Supplementary Fig. 14c; Supplementary Dataset 12). Overall, our results support the hypothesis that a vigorous plant genotype harbours a rhizosphere with a functionally more diverse microbiome, which results in improved plant performance of an underperforming genotype.

Plant-derived flavones mediate specific variations of rhizosphere bacterial taxa affecting nitrogen capture from the soil

To test if the presence of flavonoids alters rhizosphere-associated microbiota, we compared the performance of C2 wild type plants with the naturally silenced dominant maize mutant *C2-Idf* (*Colorless2-Inhibitor diffuse*), defective in a gene encoding a chalcone synthase (Fig. 3a). *C2-Idf* mutants displayed highly reduced levels of apigenin-related flavonoids in comparison to C2 wild type plants[38]. After three weeks of growth in nitrogen-poor and unsterilized soil, *C2-Idf* plants showed severe chlorosis and necrosis that progressed from older to younger leaves, which is indicative for nitrogen deficiency (Fig. 3b) and growth suppression of the shoot (Fig. 3c). After sterilization of the soil, both genotypes grew similarly weak without differences in biomass production (Fig. 3c). Next, we transplanted C2 wild type and *C2-Idf* mutant plants to soil, in which these two genotypes were grown before and observed that nitrogen deficiency symptoms of leaves were reduced in *C2-Idf* mutants planted in C2-grown soil (16 days after transplantation) (Fig. 3d). In contrast, nitrogen deficiency became more severe in C2 wild type plants that were transplanted into soil in which *C2-Idf* mutants were grown in comparison to C2 wild types which were replanted into soil in which C2 wild types were grown (20 days after transplantation) (Fig. 3d). These results suggest that the microbiota in soil, in which flavonoid-producing plants were grown, is able to alleviate symptoms of nitrogen deficiency (Fig. 3d, e). We therefore propose that flavonoids have triggered the observed promotions in plant growth and nitrogen use by changes of microbial communities. To address this hypothesis, we externally applied different types of flavonoids at different concentrations to a paper roll system and to soil, respectively, and evaluated *C2-Idf* plant performance. After all, the flavone apigenin at an optimal concentration of 1 µM for soil application was determined in the paper roll system (Supplementary Fig. 15a and b). Supplementation of different types of flavonoids at 1 µM to *C2-Idf* seedlings had no effects on shoot growth in the paper roll system (Supplementary Fig. 15c) or in sterilized soil (Supplementary Fig. 15d). This suggests that the addition of flavone had no effect on *C2-Idf* growth in the sterile system.

Notably, apigenin was the only flavone which restored growth and nitrogen accumulation for *C2-Idf* plants in unsterilized nitrogen-poor soil in contrast to other flavonoid types (Supplementary Fig. 15d and e). This suggested that the flavone-dependent rhizosphere microbe-driven processes rather than root exudate-derived flavones themselves affected plant growth and nitrogen nutrition. In addition, we examined the bacterial community of C2 wild type and of the mutant *C2-Idf* by 16S rRNA sequencing and we found that the C2 wild type rhizosphere recruited an exceptionally high abundance of the taxon *Massilia* belonging to *Oxalobacteraceae* from the phylum *Proteobacteria* (Fig. 3f, g; Supplementary Dataset 13). Sequencing of the bacterial 16S rRNA diversity in the rhizosphere of the *C2-Idf* mutant supplied with different types of flavonoids in nitrogen poor soil demonstrated that flavonoids reshape the rhizosphere microbiome (Fig. 3h). Moreover, the *C2-Idf* mutant significantly enriched *Massilia* at the genus level and *Oxalobacteraceae* at the family level in apigenin-supplemented soil in comparison to the other flavonoid types (Fig. 3i; Supplementary Dataset 14). Taken together, these results show that plant-derived flavones are likely sufficient to drive the accumulation of specific microbial taxa, affecting plant growth and nitrogen nutritional status from nitrogen-poor soil.

Flavone-conditioned rhizosphere microbiota is sufficient to recover *lrt1* performance

Lateral roots and root hairs are the major components of the root system responsible for water and nutrient uptake along the longitudinal axis of the root. Thus, we hypothesized that lateral root and root hair formation might influence microbiome differentiation along the root. Root phenotyping experiments were performed using maize mutants defective in lateral root and root hair formation under the same nitrogen-poor soil conditions. In brief, the mutants *lrt1* and *rum1* are lateral root defective. The mutant *lrt1* does not form lateral roots on the primary and seminal roots, while *rum1* does not form lateral roots on the primary root and is in addition devoid of seminal roots. The mutant *rth6* is specifically affected in root hair elongation in all root types during the whole growth period. Moreover, *rtcs* is deficient in the initiation of all seminal and shoot-borne roots while the remaining primary root forms lateral roots and root hairs. Results show that defects in lateral root formation but not in root hair development restricted biomass production in maize shoots (Fig. 4a). Interestingly, the shoot of lateral root mutant *lrt1* acquired more nitrogen than that of *rum1* in nitrogen-poor soil, although biomass production severely decreased in both lateral root mutants in comparison to the root hair mutants (Fig. 4b). This observation suggests that *lrt1* might have an alternative strategy to acquire nitrogen from nitrogen-poor soil. Moreover, *rtcs* mutants, which display only a single primary root with lateral roots but no seminal or shoot-borne roots, produced even more shoot biomass and accumulated more nitrogen in the leaves than *lrt1* and *rum1* (Figs. 4a, 4b). This highlights the contribution of lateral root formation to nitrogen acquisition from nitrogen-poor soil in 4-week-old plants, irrespective of seminal and crown root formation in these genotypes. Furthermore, we sterilized the soil and compared shoot biomass production between wild type, *lrt1* and *rum1* with and without microbes. Soil sterilization revealed dramatic repression of biomass production in *lrt1*, but no decrease was observed in *rum1* (Fig. 4c). A flavone profiling experiment using a hydroponic system demonstrated that the *lrt1* mutant produces and releases more of the two flavones apigenin and luteolin to the rhizosphere than the respective wild type (Fig. 4d). In contrast, neither apigenin nor luteolin was detected in extracts and exudates of the *rum1* mutant (Fig. 4d). To investigate

whether flavone-conditioned rhizosphere microbiota are able to impact growth and development of maize roots, we performed rhizosphere transplantation experiments with the lateral root defective mutants *lrt1* and *rum1* using nitrogen-poor soil (Fig. 4e). Interestingly, biomass production and nitrogen accumulation of *lrt1* in flavone conditioned (787 or C2 wild type grown) soil was promoted in comparison to *lrt1* transplanted into *lrt1*-grown soil, but this stimulation effects of plant performance appeared to be *lrt1*-specific (Figs. 4e, 4f). Therefore, soil sterilization together with rhizosphere transplantation results highlight important roles of flavone-conditioned microbiota on the growth performance and nitrogen uptake of the lateral root defective *lrt1* mutant plants.

Effects of *Oxalobacteraceae* isolates on lateral root formation and plant growth depend on LRT1

To investigate whether genetically determined defects in lateral root and root hair formation result in alternative rhizosphere microbiota, 16S rRNA gene amplicon sequencing was performed to profile the rhizosphere microbiota along the three developmental zones of wild type B73, the lateral root defective mutants *rum1* and *lrt1* and the root hair defective mutant *rth6* in nitrogen-poor soil (Supplementary Fig. 16a). The mutant *rtcs* was also introduced to evaluate whether seminal roots also affect the microbiota in comparison to *rum1*, which also lacks seminal roots. The lateral root defective mutants *rum1* and *lrt1* attracted similar numbers (ca. 230 OTUs) of genotype-specific bacterial taxa differing from *rth6* (170 OTUs) and *rtcs* (376 OTUs) (Supplementary Fig. 16b). Moreover, β-diversity of these mutants demonstrated separate clustering between lateral root defective mutants and root hair or seminal root defective mutants, which suggests that during lateral root formation different microbiomes are recruited in comparison to root hair or seminal root formation (Supplementary Fig. 16c). Considering that root hairs are a key component of rhizosphere formation, it was not surprising that root hair formation was an important factor for maintaining the bacterial diversity in comparison to lateral root formation (Supplementary Fig. 16d). Interestingly, in comparison to the wild type B73, the differences of bacterial α-diversity in the rhizosphere along the different zones is not reduced for the lateral root mutants *lrt1* and *rum1*, but in the root hair mutant *rth6* (Fig. 5a). This demonstrated that lateral roots are an important trigger for maintaining the spatial pattern of bacterial diversity in the rhizosphere along the developmental zones of maize crown roots. Closer inspection of specifically enriched bacterial taxa revealed distinct mutant-specific microbiota variations (Fig. 5b) and the taxon *Oxalobacteraceae* was specifically enriched in *lrt1* mutant (Fig. 5b; Supplementary Fig. 16e). Lateral root formation of *lrt1* was significantly induced by the flavone-conditioned (C2 or 787 grown) rhizosphere microbiota (Fig. 5c). Specific enrichment of *Oxalobacteraceae* in *lrt1* coincides with the finding with C2 (Fig. 3h) and the vigorous inbred lines 787 (Fig. 2c), supporting the hypothesis that specific microbial taxa might be linked with important functions related to growth promotion and nitrogen uptake in *lrt1* mutant.

To assess the functional effects of *Oxalobacteraceae* isolates on growth promotion, we applied 16 strains belonging to *Collimonas*, *Duganella*, *Herbaspirillum*, *Janthinobacterium*, *Massilia*, *Pseudoduganella* from the *Oxalobacteraceae* isolated from different soil types to the soil where *C2-Idf* mutant grew in nitrogen-poor soil (Supplementary Dataset 15). Specifically, 16S reads of C2 and the *C2-Idf* mutant were mapped to those 16 *Oxalobacteraceae* isolates, confirming that the rhizosphere of C2 plants was significantly enriched (11 out of 16 strains) in *Oxalobacteraceae* than its mutant *C2-Idf*

Discussion

Understanding the growth and development of plant roots and their adaptation to specific environmental challenges is a prerequisite for the management of nutrient inputs in sustainable agriculture. Interactions between roots and their rhizosphere microbiota are essential for plant growth and performance[7,8]. It is known that dynamic patterns of the root transcriptome synchronize with distinct microbial taxa colonizing different root types[26,27]. However, numerous scenarios and mechanisms by which microbes modulate plant development are still unknown especially in crops[44]. Our large-scale field-study in maize demonstrated that different longitudinal root zones representing distinct phases of development recruit distinct rhizosphere microbiome communities, which are associated with specific transcriptome signatures during root differentiation (Fig. 1). Synchronization of root transcriptome and rhizosphere microbiome is reflected by dynamic root exudation profiles with different compositions along the root developmental zones[3]. Our data suggest that the developmental status or function of root zones has a considerable impact on the establishment of their rhizosphere microbiome. Indeed, the transport rate of nutrients to the shoot varies between different developmental root zones[45,46], while in turn, localized edaphic factors strongly affect root hair and lateral root formation to increase the uptake of nutrients from the soil[47]. Based on the strong impact of nitrogen on root system architecture[16,48], lateral root proliferation along the parental root of maize may also favour nitrogen foraging in nitrogen-poor soil[49,50]. This suggests that causal interactions of specific root zones with the rhizosphere resulted in co-adaptation of roots and their microbiota during development. Intriguingly, bacterial diversity in the rhizosphere microbiome significantly decreases along the developmental zones of roots as illustrated by the two monogenic maize mutants *rum1* and *lrt1* with defective lateral root development (Fig. 4; Supplementary Fig. 15). This suggests that lateral roots themselves or their exudation profiles are likely a functional determinant of rhizosphere microbiome composition.

Plants can release up to 20-40% of their photoassimilate-derived carbon via their roots as exudates[51]. This is critical for shaping the rhizosphere microbiota[52]. Recent findings demonstrated that plant-derived coumarins contribute to the reshaping of the specific microbial composition under iron deficiency in Arabidopsis[53,54]. Specific metabolites such as benzoxazinoids have been demonstrated to confer root type-specific changes of microbial communities in maize[28,33]. Thus, the specific metabolite composition of the host roots can considerably influence the establishment of the rhizosphere microbiota and the enrichment of specific taxa. In the present study, correlation-based network analyses identified the flavone synthase encoding gene *FNSI2* as a hub gene, which displays very strong associations with specific bacterial taxa (Fig. 2; Supplementary Dataset 11). Targeted metabolite profiling in root extracts and exudates together with ^{14}C labelling of exudates in the rhizosphere suggest, that flavone biosynthesis and subsequent secretion might trigger the functional interactions between host roots and rhizosphere microbes thus improving plant performance (Fig. 2; Supplementary Fig. 13). Our studies on a specific mutation in the chalcone synthase-encoding gene *Colorless2* (*C2*)[38] together with rhizosphere transplantation experiments including both inbred lines and mutants demonstrated that flavone biosynthesis might be involved in the predominant enrichment of *Oxalobacteraceae* in the maize rhizosphere (Figs. 2 and 3). These experiments support the notion that the host genotype considerably influences the assembly of the rhizosphere microbiota through root-derived flavones. In this context,

secreted flavones stimulate the enrichment of the bacterial taxa *Oxalobacteraceae* in the maize rhizosphere and thus growth and nitrogen acquisition in nitrogen-poor soil. These findings also suggest that plant genotype-specific tailoring of the rhizosphere microbiota is driven by selection and coadaptation of soil-borne microbes through molecular mechanisms including root exudation[6,55].

The progressively enhanced relative abundance of *Oxalobacteraceae* from soil via the rhizosphere to the root suggests its potential association with host plant performance in Arabidopsis, barley and maize[9,56,57]. Integration of metabolite profiling of root extracts and exudates together with rhizosphere microbiome analysis of the maize mutants *lrt1* and *rum1* defective in lateral root formation, demonstrated a causal role of *Oxalobacteraceae* in maize growth and nitrogen accumulation (Figs. 4 and 5). A series of inoculation experiments confirmed consistent growth promotion and nitrogen uptake effects on *lrt1* mutants by independent soil-derived *Oxalobacteraceae* isolates belonging to the genus *Massilia* (Fig. 5). Flavonoid biosynthesis genes were specifically enriched in differentiated root zones with emerged root hairs and lateral roots[58]. In fact, *Massilia* preferentially colonize the mature parts of the root in comparison to the growing root tip[59]. This highlights that flavonoid biosynthesis-related genes might represent important players impacting root development while interacting with rhizosphere microbes. It has been demonstrated that growth-promoting rhizobacteria are able to modulate primary root development[17,60,61] but also lateral root formation[62]. Production and signalling of auxin[61-63] are well-defined mechanisms by which bacteria modulate plant root development in Arabidopsis. Notably, both flavone-enriched rhizosphere microbiota and *Oxalobacteraceae* strains can only rescue the growth and formation of lateral roots in the mutant *lrt1* but not in the auxin-signalling defective mutant *rum1* of maize (Figs. 4 and 5). However, *Oxalobacteraceae* strains did not *in vivo* produce indolic compounds such as IAA, indolepyruvic acid and indoleacetamide or display root auxin induction effects using *DR5::GUS* reporter lines in Arabidopsis (Supplementary Figs. 17 and 18). These results suggest that in *lrt1* a specific microbe-mediated pathway alters the balance between proliferation and differentiation during lateral root development, most likely independent of bacteria- and plant-derived auxin-related processes in maize (Fig. 6). Recent studies highlight that shared molecular networks could have evolved through the interplay between rhizobia-mediated nodulation and lateral root development[64-66]. Together, these findings indicate that an LRT1-mediated molecular component that guides plant developmental processes also coordinates the engagement of host roots with microorganisms under nitrogen deprivation. It is important to point out that we performed metabolite profiling and rhizosphere transplantation only for one pair of genotypes (787 and LH93), which is not representative for all maize genotypes. Further studies are needed to investigate whether the effects of growth promotion and nitrogen uptake derived from *Oxalobacteraceae* are also observed in other maize genotypes. Nevertheless, our subsequent genetic studies using an independent flavonoid biosynthesis mutant *C2-Idf* together with root defective mutant *lrt1* provided consistent results. Moreover, we will survey how the evolutionary conservation of developmental plasticity is conferred by the rhizosphere microbiota in plants. Future studies need to disentangle the complexity of bacteria-bacteria interaction mediated by host-derived metabolites and how this will influence the architecture and function of the root system under nutrient deprivation.

In summary, our data indicate that developmentally controlled biological activities in maize roots are critical for the beneficial interactions with the rhizosphere microbiota. Under nitrogen deprivation, maize assembles specifically bacteria of the taxon *Oxalobacteraceae* in the rhizosphere. This in turn facilitates nitrogen capture through modulation of lateral root development. A full understanding of the causal relationships between the rhizosphere microbiota, host gene regulation and genetic variation controlled by root development could pave the way for new approaches towards securing high crop yield in a sustainable agriculture. Based on our results, the re-introduction of alleles coding for beneficial flavones into elite maize lines might improve favourable interactions between the root system and its growth promoting rhizosphere biota in maize. Hence, maximization of beneficial plant-microbe interactions as a selection target is a promising strategy for breeding of high-yielding and nutrient efficient crops.

Materials and Methods

Field and phytochamber experimental design and maize genotypes

In spring 2018, 72 maize inbred lines from the US Ames panel[67] were hand planted in a randomized complete block design with three biological replications in the field of the long-term experimental station of China Agricultural University located in Quzhou, China (36.52 N, 115.02 E) (Supplementary Fig. 19a). The cropping system on this field plot is a winter wheat - summer maize rotation each year, which is representative of the typical cropping system on the North China Plain. In this long-term field plot no synthetic fertilizers has been applied in the last 30 years. The basic nutrients of the alluvial loamy soil from the whole plots were measured for the top 30 cm soil before sowing (Supplementary Table 4). Prior to fertilization and planting of the field experiment, we collected bulk soil samples from the different field plots (Supplementary Fig. 19a) and verified homogeneous distribution of bacterial diversity across the field by bacterial 16S rRNA sequencing (Supplementary Fig. 19b). This enabled us to examine stable patterns of rhizosphere microbiota between genotypes and root zones under the conditions of our field. The field was sufficiently irrigated one month prior to sowing to keep proper soil moisture for maize growth. Before sowing of this field experiment, straw from the previous season was removed from the field and 75 kg P ha^{-1} (as calcium superphosphate), 75 kg N ha^{-1}(as urea) and 75 kg K ha^{-1} (as potassium sulfate) were applied and mixed with the surface soil by rotary tillage to meet plant needs for 4-week-old maize. Planting density of all maize inbred lines was approximately 67,500 plants ha^{-1} with a row width of 60 cm. Precipitation and irrigation, solar radiation and daily average temperature were recorded and no herbicides or pesticides were applied during the growth period (Supplementary Fig. 20).

Of the 72 maize inbred lines, 20 inbred lines, which performed particularly well under the given field conditions were selected for follow-up experiments. These inbred lines represented seven distinct clades (A to G, Supplementary Fig. 1a) of a phylogenetic tree: Clade A (LH38, LH39, 78371A), Clade B (IB014, PHJ75, PHM10, PHN11), Clade C (A632, B73, LH205, PHW51), Clade D (E8501, LH51, LH52, Mo17), Clade E (LH93), Clade F (PHJ31, PHW20) and Clade G (787, W64A).

For the phytochamber pot experiments, the described inbred lines and segregating lines of the monogenic maize root mutants *lrt1* (*lateralrootless 1*), *rum1* (*rootless with undetectable meristem 1*), *rth6* (*roothairless 6*) and *rtcs* (*rootless concerning crown and seminal roots*) and their wild type B73 have been pre-germinated for three days in a paper roll system with distilled water and then transferred to soil filled pots (7 cm × 7 cm × 20 cm) in a 16-h-light, 26 °C, and 8-h-dark, 18 °C cycle. Plants were daily watered to maintain optimal conditions for maize growth. No additional fertilizer has been added during maize growth. The phenotypes of those mutants have been described[19]. Finally, homozygous naturally silenced maize *C2-Idf* (*Colorless2-inhibitor diffuse*) mutants and the corresponding C2 wild type maize seeds were surveyed[68]. The *Colorless2* (*C2*) gene encodes a chalcone synthase, which produces flavones in kernels of pigmented C2 wild type plants[38].

Determination of aboveground traits in the field

Aboveground traits were examined for all 20 inbred lines on the day of harvest in the field. The complete aboveground part of the plant was harvested and the dry biomass was determined. Leaf length (L) and width (W) were measured at harvest and leaf area (A) was calculated as A = L × W × K, where K = 0.75 was used for fully expanded leaves and K = 0.5 was introduced for incompletely expanded leaves[69]. Leaves were defined as fully expanded if a ligule was formed. A leaf was considered to have senesced when half or more of its area had yellowed. Chlorophyll content was determined as average of 30 measurements with a SPAD-502 chlorophyll meter (Konica Minolta, Ramsey, NJ, USA) in the middle third of the leaf in longitudinal direction. Dried shoot samples were ground and nitrogen concentrations were determined with a modified Kjeldahl digestion method[70] from 0.2 g of plant material.

Sampling of root and rhizosphere soil in the field and phytochamber

The root and rhizosphere samples were harvested from 28-day-old maize plants in the field. At that time, all nutrients from the seed had been consumed by the seedling growth. Hence, distinct seed sizes do not have any impact on root exudation in different genotypes. Irrigation of the field was terminated 3 days before sample collection to facilitate the rhizosphere harvest. For each genotype, root systems were carefully dug out to a depth of ~40 cm depth using a spade and all genotypes started to form the 3rd whorl of crown roots and the 2nd whorl of shoot-borne crown roots of a length of ca. 7 cm were selected (Fig. 1b). Two to three crown roots formed at the 2nd whorl shoot node in all 20 genotypes. We sampled root systems of six random plants from the center of each plot to avoid border effects. Three of the six sampled root systems with clear and integral whorls of crown roots were subjected to root and rhizosphere harvesting. To this end, the whole root system was gently shaken to remove the big soil particles leaving soil attached to the roots defined as the rhizosphere[71]. Subsequently, only the 2nd whorl of the crown roots from all three plants was dissected into three developmentally distinguished zones. Due to the differential availability of root exudates, it has been proposed that the role of rhizosphere microorganisms for nutrient uptake varies along the root[3]. Thus, we separated the longitudinal root zones according to their distinct developmental characteristics, reflecting dynamic root nutrient uptake rate, exudation rate and microbial turnover (Fig. 1a). It should be noted that the boundaries between the different root zones are gradual, thus the separation strategy is mainly based on the emergence of root hairs and visible lateral roots. First, 5 mm comprising the root cap and the meristematic zone were removed because there was no rhizosphere soil attached in this region of the root. The boundary between elongation zone and differentiation zone was defined by emerging root hairs, which are characteristic for the differentiation zone. Zone 1 was defined as the meristematic zone and apical part of elongation zone comprising the region of ~0.5-2 cm measured from the tip which did not contain any root hairs for all genotypes. Zone 3, was defined as the basal part of the differentiation zone and comprised the ~4-7 cm of the crown roots from the root tip with root hairs and emerged lateral roots. Finally, zone 2 was harvested, which is defined as the remaining segment between zones 1 and 3 covering the basal part of the elongation zone and apical part of differentiation zone with root hair and lateral root primordia formation comprising the region ~2-4 cm from the root tip. All dissecting steps for root zones have been performed by the same person on ice with sterilized blades in a customized tent on the field site to avoid systematic errors. For each biological replicate per root zone and genotype,

samples of two to three crown roots of three plants resulting in six to nine crown root segments were pooled. Bulk soil samples across each of the plots were taken in the middle between maize rows at a depth of 30 cm. All root samples were packed in aluminium foil and were immediately frozen in liquid nitrogen and stored at -80 °C before extraction of rhizosphere soil. To guarantee high quality root RNA from the field samples, the sampling steps were repeated for additional three plants and the rhizosphere soil was immediately washed away by a Pressure Washer (XM-2081A, Panda Group, Shanghai, China). Subsequently, these roots were separated into three corresponding zones for transcriptome analyses as described above. The pooled zone-specific root samples were dried by clean tissue, wrapped in aluminium foil and were then immediately frozen in liquid nitrogen and stored at -80 °C before RNA extraction. For the experiment in the phytochamber, the mutant rhizosphere samples were harvested as described above. Because of lateral root (*rum1* and *lrt1*) and root hair (*rth6*) defects, the zone-specific segments of the mutants were defined according to the length of their corresponding zones of the wild type seedlings.

Extraction of root zone-specific rhizosphere samples in the lab

Rhizosphere samples in this study are defined as the combination of the “rhizosphere” and “rhizoplane” compartments[71]. Frozen rhizosphere samples were extracted from the corresponding root segments according to established protocols[9]. In brief, the frozen samples were thawed to room temperature and placed into a 50 ml falcon tube with 20 ml sterile PBS buffer (pH 7) amended with 0.02% Silwet L-77 (Sigma). The falcon tubes with samples were shaken for 20 min with 35 rpm by a cycle agitator (NeoLab). Subsequently, those roots were transferred to a new falcon tube containing 20 ml of PBS-Silwet L-77 solution and the shaking step was repeated twice. Afterwards, the rhizosphere samples were centrifuged for 20 min at 4000 *g* at a temperature of 16 °C. This step was repeated twice. Then the supernatant was removed and 300 µl of sterile water was added to re-suspend the soil. Finally, the rhizosphere soil (lysing matrix) was transferred into a 1 ml tube and the samples were frozen in liquid nitrogen and stored at −80 °C before DNA extraction.

Total RNA isolation from root zone samples

For transcriptome analysis, the three biological replicates of frozen root samples across the three longitudinal zones were ground in liquid nitrogen. Total RNA was isolated by the RNeasy Plus Universal Mini Kit (Qiagen). RNA quality was assessed by agarose gel electrophoresis and by an Agilent RNA 6000 Nano LabChip in an Agilent 2010 Bioanalyzer (Agilent Technologies). All RNA samples were with high quality as documented by RNA integrity number (RIN) values higher than 6.0. During the quality control steps, an Agilent DNA 1000 LabChip (Agilent Technologies) and an ABI StepOne Plus Real-Time PCR System (Applied Biosystems) were used for quantification and quality control of the sample libraries. The cDNA libraries for RNA-seq were constructed with a TruSeq RNA Sample Prep Kit (Illumina). Cluster preparation and PE150 read sequencing were performed according to the Novaseq 6000 guidelines (Illumina).

Transcriptome profiling by RNA-seq and raw sequencing data analysis

were carried out with Phusion High-Fidelity PCR Master Mix (New England Biolabs) according to the manufacturer's instructions. Subsequently, PCR reactions were mixed with 1× loading buffer (containing SYB green) and separated on 2% agarose gels. PCR products with the brightest band between 400-450 bp were chosen for further experiments. PCR products were mixed in equal density ratios and were subsequently purified with the Qiagen Gel Extraction Kit (Qiagen, Germany). Sequencing libraries were generated using the NEBNext® Ultra DNA Library Pre Kit for Illumina, following the manufacturer's recommendations and by adding sequence indices. The library quality was assessed on the Qubit@ 2.0 Fluorometer (Thermo Scientific) and Agilent Bioanalyzer 2100 system. Finally, the library was sequenced on an Illumina HiSeq 2500 platform (Illumina Inc., San Diego, USA) and 250 bp paired-end reads were generated at the Novogene Bioinformatics Technology Co., Ltd. (Beijing, China).

16S rRNA gene and ITS1 read data processing

Paired-end 16S rRNA amplicon sequencing reads were assigned to samples based on their unique barcode and truncated by cutting off the barcode and primer sequence. Paired-end reads were merged using FLASH (v1.2.7)[76] and the splicing sequences were called raw tags. Quality filtering on the raw tags were performed under specific filtering conditions to obtain the high-quality clean tags according to the QIIME (v1.7.0) quality controlled process[77,78]. Raw tags were compared with the reference Gold database using the UCHIME algorithm (v7)[79] to detect chimera sequences, which then were removed to obtain the effective tags[80]. Sequence analyses were performed by Uparse software (v7.0.1001) and only sequences with ≥97% similarity were assigned to the same OTUs[81]. For each representative sequence for each OTU, Mothur software was performed against the SSUrRNA database of SILVA Database (release 128)[82] for species annotation at each taxonomic (kingdom, phylum, class, order, family, genus, species) rank (threshold 0.8-1)[83]. Mitochondria- and chloroplast-assigned OTUs were eliminated. Out of the remaining sequences an OTU table was built (only reads >2 copies were retained). In order to study phylogenetic relationships of different OTUs and differences of the dominant species in different samples (groups), multiple sequence alignments were conducted using MUSCLE software (v3.8.31)[84]. Those sequences that did not align were removed. ITS amplicon data were processed as following: reads were merged, demultiplexed and filtered as described in the previous section and then dereplicated and sorted keeping only those with >2 copies. Subsequently, sequences with ≥97% similarity were assigned to the same OTUs using UCLUST (v7). We picked a representative sequence for each OTU and used the UNITE Database[85] to annotate taxonomic information based on a BLAST algorithm which was calculated by QIIME (v1.7.0). OTU abundance information for bacteria and fungi were normalized using a standard of sequence number corresponding to the sample with the least sequences. Subsequent analysis of α-diversity and β-diversity were all performed based on this output normalized data.

Calculation of α- and β-diversity of microbiome

In order to compute α-diversity, we rarefied the OTU table and calculated the Shannon's diversity index estimated as the diversity found in each sample with QIIME (v1.7.0) and displayed this data with R

software (v2.15.3). We performed β-diversity analyses to evaluate differences of samples in species complexity. β-diversity on both weighted and unweighted unifrac were calculated by QIIME (v1.7.0). We then performed a principal component analysis (PCA), which was applied to reduce the dimension of the original variables using the FactoMineR package and ggplot2 package in R software (v2.15.3) followed by a cluster analysis[86]. A distance matrix of weighted or unweighted unifrac among samples obtained before was transformed to a new set of orthogonal axes, by which the maximum variation factor is demonstrated by first principal component, and the second maximum by the second principal component, and so on. The Unweighted Pair-group Method with Arithmetic Means (UPGMA) clustering was performed as a type of hierarchical clustering method to interpret the distance matrix using average linkage and was conducted by QIIME software (v1.7.0). Tukey's *post-hoc* ANOVA tests and two-tailed Student's *t*-tests were conducted to determine the microbial diversity of the different zones. The relative abundances of microbial taxa among root zones and genotypes were determined and statistical analyses were based on FDR-corrected Kruskal-Wallis test (p <0.05). Linear discriminant analysis (LDA) effect size (LEfSe) method was applied to differentiate specific bacterial taxa in the rhizosphere of the developmental defective maize mutants. For LEfSe, Kruskal-Wallis and pairwise Wilcoxon tests were performed, followed by LDA to assess the effect size of each differentially abundant taxon[87]. In this study, a p-value of <0.05 was considered significant for both statistical methods. Bacteria with markedly increased numbers were defined as those with an LDA score ($\log_{10}$) of over 2.

Microbial OTU-based correlation network construction

To evaluate the effects of zone and genotype specificity on microbiome composition, two correlation networks were individually constructed for bacteria and fungi respectively[88]. OTU tables for each dataset were restricted to OTUs comprising >200 reads for all 180 samples and produced 5,232 bacterial and 1,439 fungal operational taxonomic units OTUs (Supplementary Dataset 7). For each table, Spearman correlation scores were calculated using the CoNet app (v1.1.1.beta)[89] for Cytoscape (v3.7.0)[90]. Negative edges were discarded, and only edges with correlation scores of >0.6 were kept (p <0.05, Bonferroni-corrected). To this end, the proportion of inter-taxa and intra-taxa edges (using the edge weights) was calculated for each of the occurring node affiliations. To construct interkingdom co-occurrence networks, the raw read count tables for the 16S and ITS datasets were merged to give one table per genotype by zone. OTUs that appeared in less than ten samples were removed. These filtered interkingdom tables were used as an input for SparCC (Python v3.5.2 and numpy v1.11.0)[91]. The analysis was conducted with default parameters and 100 bootstrap samples were used to infer pseudo-p-values. The inferred correlations were restricted to those having correlations >0.6 and <-0.6 (p <0.05, two-tailed). Within the networks, proportions of inter- and intra-taxa edges were calculated. Intra-taxa refer to edges within bacterial OTUs and fungal OTUs, whereas inter-taxa refer to edges between these groups. The cumulative bacterial or fungal correlation refers to the sum of all intra-taxa correlations for each fungal and bacterial OTU. Visualization of the networks was done with Cytoscape (v3.7.0) as well.

Covariance analysis of plant-microbe (Gene-OTU) and bacteria-fungi (bOTU-fOTU) interaction

To fully capture whether our high dimensional data sets of transcriptome and microbiome have the covariance components into genotypes and developmental zones, raw RNA-seq reads for 39,179 protein-coding genes and 180 samples (x, genotypes; y, root zones; z, replications) were filtered for extremely lowly expressed genes, excluding 4,213 genes with a sum of less than ten reads across all samples thus keeping 34,966 genes. To include only genes and OTUs (bOTUs and fOTUs) in the final analysis, which show variation for one of the factors genotype, zone or genotype-by-zone interaction, we pre-filtered the sets of genes, bOTUs and fOTUs separately. This pre-filtering was done by assessing significance of the three factors, mentioned before, for each gene or OTU, using an analysis of variance (R function aov()) with the model:

gene expression ~ genotype + zone + genotype:zone,

OTU abundance ~ genotype + zone + genotype:zone,

where genotype represents the x genotypes, zone represents the y root zones, and genotype:zone the interaction of both effects. We adjusted significance *p*-values using the R function p.adjust() with method = "BH" for Benjamini-Hochberg which corresponds to the FDR and adjusts *p*-values according to the number of observations. Genes or OTUs with an FDR <0.05 in at least one of the three factors were kept, all other genes or OTUs were filtered out.

In total, 27,092 pre-filtered genes were used as input to identify differentially expressed genes for each OTU (bacterial and fungal) by using the R package DESeq2 (v1.18.1) with the model gene expression ~ OTU abundance. OTU abundance was taken as a trait to explain gene expression. Significant genes were determined with corresponding bOTUs and fOTUs with FDR and $\log_2$ fold change for α levels of 0.001. Moreover, we performed the same analysis as above but explaining bOTU abundance with fOTU abundance

bOTU abundance ~ fOTU abundance

and *vice versa*

fOTU abundance ~ bOTU abundance,

in order to identify direct associations between fungal OTUs and bacterial OTUs.

Network-based integration of host transcriptome and rhizosphere metagenome

Network-based analysis is the most biologically interpretable tool to analyse the dependency among variables, such as relationships between microbial compositions and gene expressions[92]. The WGCNA is a data-driven method, which discovers the co-clustered gene sets (modules) based on weighted correlations between gene transcripts[93]. To understand how functional changes of host transcriptome associate with the environmental variations of microbial taxa along the longitudinal axis of root, we performed WGCNA to identify the correlations among quantitative data sets using R package: (i) gene co-expression modules among 20 maize lines across three longitudinally distinct zones and (ii) module eigengene value-microbial taxa associations and intra-modular hub genes. WGCNA is designed to be an unsupervised analysis method that clusters genes based on their expression profiles for our 180

genotype-zone specific samples. To robustly construct co-expression networks, only genes with mapped reads ≥5 at least for one genotype with corresponding zones and differentially expressed genes between genotypes/zones generated by CLC Genomics Workbench were kept. The gene expression was normalized according to Log_2 (FPKM+1) expression. The soft thresholding power β calculated adjacencies. To minimize the effects of noise and false associations, we transformed the adjacencies into a topological overlap matrix (TOM), and calculated the corresponding dissimilarities (dissTOM) as 1 - TOM. To hierarchically cluster the genes, we used dissTOM as a distance measure and set the minimum module size (number of genes) to 30 to detect modules. To quantify the co-expression similarities of entire modules, the eigengenes of modules were calculated and clustered based on their correlation and subsequently used to study the crosstalk between functional transcripts and microbial traits[94]. We chose the correlation of 0.9 to cluster the modules. The modules' eigengenes were used to represent the gene expression patterns within a module[93]. Annotation of co-expressed genes within modules was analyzed by AgriGO. The GO terms were further imported to the online tool REVIGO to identify the most connected and represented GO terms[95]. Cytoscape (V3.7.0) will be used to visualize the co-expression network and most connected GO terms.

The relative abundance of the rarefied bacterial and fungal OTU table with taxonomic information was further imported into the WGCNA data frame and each classified taxon was treated as a "physiological trait". The module eigengene was correlated with these microbial traits for the most significant associations. Pearson correlations and their associated *p*-values were then generated for all pairwise comparisons of the module eigengene expression values across the 20 genotypes with three zones. Bonferroni adjustments corrected for multiple comparisons. The modules exhibiting high correlations with microbial taxa were further studied to identify: (i) overrepresented GO categories; and (ii) highly connected module 'hub' genes related to microbial taxa. The highly correlation modules/eigengenes with microbial taxa was visualized by Cytoscape (v3.7.0) as described above.

Shotgun metagenomic analysis

In addition to taxonomic composition, we performed a shotgun metagenomic sequencing to gain insights into the functional differences between 787 and LH93 rhizosphere microbiomes. A total of three 787 and three LH93 rhizosphere samples were randomly selected from 4-week-old plants in the phytochamber. The isolated DNA integrity and purity was controlled by 1% agarose gel electrophoresis and NanoPhotometer® spectrophotometer (IMPLEN, CA, USA). DNA concentration was accurately quantified by Qubit® dsDNA Assay Kit in Qubit® 2.0 Flurometer (Life Technologies, CA, USA). For each sample, 1 μg of genomic DNA was used with Illumina's TruSeq for library generation using NEBNext® Ultra™ DNA Library Prep Kit for Illumina (NEB, USA). Briefly, the DNA sample was fragmented by sonication to a size of 350 bp, then DNA fragments were end-polished, A-tailed, and ligated with the full-length adaptor for Illumina sequencing with further PCR amplification. At last, PCR products were purified (AMPure XP system) and libraries were analysed for size distribution by Agilent 2100 Bioanalyzer and quantified using real-time PCR. The clustering of the index-coded samples was performed on a cBot Cluster Generation System according to the manufacturer's instructions. After

cluster generation, the library preparations were sequenced on an Illumina HiSeq 4000 platform and 150 paired-end reads were generated.

For the bioinformatics steps, raw FASTQ sequences were filter-trimmed to remove the adapter sequences, low quality reads and the host genome sequences using readfq, fqcheck, soap2.21 and bwa-0.7.10. Samples passing quality check were assembled initially using an optimized MEGAHIT (K-mer = 55) and mapped to assembled scaftigs using Soap 2.21 and unutilized pair-end reads were collected. Mixed assembly was conducted on the unutilized reads with the same assemble parameter. The scaftigs of each sample and mixed assembled, which were less than 500 bp, were trimmed. And the effective scaftigs were used for further analysis and gene prediction. PCA analysis was used for the dimension reduction analysis. Functional annotation was performed by comparison of quality-filtered reads to annotated ones using COG databases[96] (Release clovr-1.0-RC9).

Flavone quantification in root extracts

Root extracts were prepared from 5-50 mg of lyophilized and ground material using twice 1 ml 70% methanol containing 1% formic acid and once 1 ml 100% ethanol-containing 1% formic acid. After addition of the extraction solvent the reaction tubes were vortexed for 30 s, sonicated for 15 min in an ultrasonic bath with cooled water and shaken for 2 h in an overhead shaker at 4 °C. After centrifugation (15,000 rpm, 30 min, 4°C), the supernatants were transferred and pooled in a 5 ml reaction tube. Extracts were dried in a Speed Vac at 45 °C. Dried samples were re-suspended in 50 µl 50% MeOH containing 0.1% formic acid. A volume of 40 µl was transferred to an UPLC vial and measured values were normalized to total root dry mass. Residual volumes from all samples were pooled, vortexed and transferred to an UPLC vial to be used as quality control sample.

Chromatographic separation was performed on a Vanquish™ UHPLC system (Thermo Fischer Scientific, San Jose, CA, USA). Flavone (apigenin and luteolin, purity ≥99%; Extrasynthese, Genay, France) baseline separation was achieved on a reversed phase Acquity UPLC® HSS T3 column (100 Å, 2.1 × 150 mm, 1.8 µm, Waters, MA, USA) using a gradient elution of A (Water, 0.1% FA) and B (ACN, 0.1% FA) as follows: 0-1 min, 10% B; 1-2 min, 10% to 30% B; 2-5 min 30% to 65% B; 5-6 min, 65% to 85% B. Additional steps were included for column rinsing and equilibration yielding a total run time of 13 min. To preserve the integrity of the separation, a guard column (130 Å, 2.1 × 5 mm, 1.8 µm, Waters) was also used. The column temperature was set to 35 °C and the flow rate to 0.3 ml/min. The injection volume was 5 µl. The UHPLC system was coupled to Q-Exactive Plus Mass Spectrometer (San Jose, CA, USA) equipped with a HESI source, operating in positive ion mode. Source values were set as follows: Spray voltage 3.5 kV; capillary temperature 320 °C; S-lens RF level 50; aux gas heater temp 400 °C; sheath gas flow rate 50; aux gas flow rate 14. For spectra acquisition a Targeted-SIM/dd-MS² experiment was performed. Resolution in Full Scan was set as 70,000. For MS/MS experiments resolution 17,500 and NCE 40 V were used. MS data were acquired and processed by Trace Finder Software (v4.1, Thermo Scientific, San Jose, CA, USA). Ten calibration solutions in the range of 1 to 800 ppb containing apigenin and luteolin standards in 50% MeOH and 0.1% FA were prepared from a stock solution of 1000 ppb. To generate the calibration

curve, the peak area on the extracted ion chromatogram (XIC) of the protonated molecule ion $[M+H]^+$ was measured. A least-square linear regression weighting by the reciprocal of the concentration was used to best fit linearity of the curve. LOQ was found to be 1 ppb. The identification of compounds found in extracts was based on the comparison of retention time, high-resolution m/z spectrum and isotope pattern with standards. Additionally, generated MS^2 spectra were searched into a custom spectral library for confirmation of the identified compounds.

Flavone quantification in root exudates in hydroponics

Seven-day-old maize seedlings in the paper roll system were transferred to the hydroponic system for another three weeks of cultivation. For exudate collection, four individual plants for each genotype (787, LH93, B73, *lrt1* and *rum1*) were pooled and rinsed thoroughly three times with sterilized distilled water. Pooled roots were then immersed into a cylinder filled with freshly sterilized water with continuous aeration for 2-h collection. Root exudates were passed through a 0.2 µm filter (Filtropur S, Sarstedt) and frozen at −20°C. The root fresh weights were recorded in parallel for normalization of the exudates. The identification of apigenin and luteolin was performed as described above. In brief, 10 ml root exudates were first lyophilized and then resuspended in 250 µl of 50% MeOH containing 0.1% formic acid. Samples were sonicated for 15 min and shaken 1 h in an overhead shaker at 4 °C. After 30 min centrifugation (15,000 rpm, 4°C), 50 µl of the supernatants were subjected to UPLC analysis and measured values were normalized to root fresh weight and root exudate collection period and thus expressed as rate.

Tracking root exudation by $^{14}CO_2$ pulse labelling and ^{14}C imaging in the soil

To understand how the carbon efflux from the root to the rhizosphere, three-day-old pre-germinated seedlings of 787 and LH93 with equal length of primary roots were transferred and grown in the rhizobox system in a phytochamber (16 h/8 h light/dark and 26 °C/18 °C) with six biological replicates. During the three weeks of maize growth, the rhizoboxes were kept inclined at an angle of 45° in order to make sure that the roots can grow along the lower side of the rhizobox. After 3-week culture, the plants were placed in an airtight chamber with an inner dimension of 1.5 m × 1 m × 1 m for $^{14}CO_2$ pulse labelling and ^{14}C imaging (Supplementary Fig 12a). The chamber was connected with a glass vial which contained 1 M NaOH before labeling. 1 M NaOH in the glass vial was used to trap the CO_2 in the chamber for 6 h. After trapping the CO_2, a new glass vial contained $Na_2{}^{14}CO_3$ was connected to the chamber and 1 M H_3PO_4 was added to the $Na_2{}^{14}CO_3$ solution through a pipe. Each plant was labeled with 0.4 MBq $^{14}CO_2$. After 6 h labeling, the remaining $^{14}CO_2$ was removed by 1 M NaOH for 1 h.

The ^{14}C distribution pattern was determined along the whole rhizobox by incubating an imaging plate (BAS-MS 2040; 20 by 40 cm; BAS-MS 2040, Fujifilm, Germany) on an open side panel of it for 22 h. The sensitive side of the imaging plate was protected with a plastic bag and was put on the soil surface. The plates were scanned by a ^{14}C imager Typhoon FLA 9500 (Perkin Elmer, Germany) at a spatial resolution of 50 µm. The digital resolution was 65,536 with 16 bit per pixel (size 0.1 mm × 0.1 mm). The ^{14}C signal was calibrated by adding ^{14}C solvent of different radioactivity (0, 100, 500, 1 MBq) to the soil in the wells of a black frame, which was then scanned in the same manner as the samples.

Images were quantified using Matlab (The MathWorks, 2015) based on the gray values (recorded intensities) at a resolution of 50 µm[97]. To quantify the ^{14}C images, the images were converted from a log into a linear system by applying the following equation:

$$PSL = \left(\frac{Res}{100}\right)^2 \times \frac{4000}{S} \times 10^{\left(\frac{QL}{G} - \frac{1}{2}\right)}$$

where *PSL* (photostimulated luminescence) is the quantified value of the image in linear scale, Res is the resolution of the image (µm; Res = 50 µm), S the sensitivity (S = 5,000), L the latitude (L = 5) and G the gradation (G = 65,535).

The vertical distribution of the ^{14}C throughout the soil profile was obtained by subtracting gray values of the frame surrounding the profile as a background. The digital scan of ^{14}C distribution across the vertical soil profile was transformed based on a color map of calibration Finally, quantification of signal intensity was calculated by the total hotspot (%) per image as area with high ^{14}C activity, then calculated the same for all six replicates and quantified as increment of hotspots (%).

Maize growth assay by flavonoid compounds in the paper roll system

To testify how flavonoid compounds affect maize growth, we applied flavone (apigenin and luteolin) and flavonol (quercetin and epigallocatechin) and investigated biomass production of *C2-Idf* mutant plants which are defective in flavonoid production in the paper roll system and soil pots. For the paper roll experiment, maize kernels were distributed in one line on the Anchor paper (length: 38 cm, width: 25 cm) at about 2 cm from the top with an interspace of 3-4 cm (Supplementary Fig. 14a). Then the paper was rolled to be sure that all kernels stay in place and the rolls with kernels were put into a 5 L beaker with 1 L deionized water for culture in the phytochamber (16 h/8 h light/dark and 26 °C/18 °C). To avoid inhibitory effects of high concentrations of flavonoids on growth, we first set up a series of induction experiment using different concentrations of apigenin ranging from 1 µM to 20 µM in the paper roll system. Suitable concentrations of apigenin were further compared with the other three flavonoid compounds to determine if different types of flavonoids have divergent effects on maize growth in the paper roll system. For application of flavonoids in the paper roll system, maize seeds were germinated and primary roots ca. 1-2 cm were selected and treated with different concentrations/types of flavonoids by spraying the solution to the whole area of root growth. Spraying treatment was applied once a day for in total seven days.

Tracking the flavonoid effects on bacterial diversity of the *C2-Idf* mutant rhizosphere in the pot experiment

To explore how flavonoids interact with soil microbiota, 1 µM of the flavonoids determined by induction experiments in the paper roll system was applied into the soil pots. In brief, the same amount of sterilized and unsterilized soil was filled until half of the soil pots and then 20 ml flavonoid solution was spread-watered into pots. The germinated three-day-old maize plants were transferred to the soil pots with the other half of the sterilized and unsterilized soil with another 20 ml flavonoid solution. The plants were grown in the phytochamber as described before and different types of flavonoid compounds were applied once a week for four weeks in soil pots. The fresh shoot biomass was determined and the 16S

rRNA gene sequencing was performed to quantify the bacterial diversity under the different types of flavonoid types in the *C2-Idf* mutant rhizosphere as described before.

Plant and soil mineral nutrients determination by elemental analyser and ICP-MS

Plant samples were heat-treated at 105 °C for 30 min, dried at 70 °C to constant weight, weighed and ground into powder. Approx. 6 mg of ground plant material was used to determine the total nitrogen concentration by using Euro Vector CHNS-O Elementalanalyser (HEKAtech GmbH-Analysentechnik, Wegberg, Germany). The data were then calculated into peak areas by the Callidus™ software providing quantitative results using reference material as a calibrating standard. The same plant samples were used to determine the concentrations of 13 additional mineral nutrients. Leaf material (ca. 10 mg) was weighed into PTFE digestion tubes and concentrated nitric acid (0.5ml; 67-69%, Bernd Kraft, Duisburg, Germany) was added to each tube. After 4 h incubation, samples were digested under pressure using a high-performance microwave reactor (Ultraclave 4; MLS, Leutkirch, Germany). Digested samples were transferred to Greiner centrifuge tubes and diluted with de-ionized (Milli-Q®) water to a final volume of 8 ml. Elemental analysis was carried out using inductively coupled plasma - mass spectrometry (ICP-MS, Sector Field High Resolution (HR)-ICP-MS, ELEMENT 2, Thermo Fisher Scientific, Dreieich, Germany) with Software version 3.1.2.242. For sample introduction a SC-2 DX Autosampler (ESI, Elemental Scientific, Mainz, Germany) was used. A six point external calibration curve was set from a certified multiple standards solution (Bernd Kraft, Duisburg, Germany). The standard reference material Tomato Leaves (NIST, 1573a) was used to verify data precision and accuracy. The elements Rodium (Rh) and Germanium (Ge) were infused online and used as internal standards for matrix correction.

Fresh soil samples were immediately frozen and stored at -20 °C for mineral nitrogen ammonium and nitrate analysis. In parallel, the same portion of fresh soil samples were air-dried and ground into powder for total nitrogen analysis. Determination of nitrogen concentration and data calculation were performed as described for plant samples.

Transplantation of maize rhizosphere in the soil pots

To investigate the influence of rhizosphere microbiota on plant growth and nutrient acquisition in maize, we examined the growth dynamics and nutritional diagnosis of maize inbred lines (787, LH93) and mutants (C2 wild type and its mutant *C2-Idf,* B73 wild type and its lateral root mutants *lrt1* and *rum1*) growing with a disturbed microbial community in the rhizosphere under the nitrogen-poor conditions. First, we compared the performance of the same genotype in natural and in sterilized soils and measured the dry biomass after one month. For soil sterilization, we first moistened the soil with sterilized water and autoclaved it in a liquid cycle for 25 min at 121 °C and left the sterilized soil at room temperature for at least 24 h. Then we repeated this procedure. After cooling down, the sterilized soil was stored at 4 °C for stabilization for at least one week and was then used for growing plants. For rhizosphere transplantation, surface-sterilized seeds of maize were germinated in the paper roll system with sterilized water and transferred into pots with natural field soil from Cologne, Germany[9]. For transplantation, the 1-month-old maize plants were carefully removed from the pot, leaving most of the

rhizosphere soils attached to the roots. This was achieved by gently crushing the soil adhering to the maize roots. The roots were then washed thoroughly in 25 ml of autoclaved deionized water by 5 min sonication in a water bath (TRANSSONIC T420, Elma, Germany) to remove most of the rhizosphere soil. The removed rhizosphere soil suspension was returned to the original pots in which the uprooted maize plants were grown. The newly germinated seeds with 1-2 cm primary roots were then replanted either into pots with the soils in which the same genotype was grown or into pots with soil in which a different genotype was grown. Plants were monitored for nutritional deficiency symptoms over time after inoculation, and nitrogen deficiency was rated as the ratio of yellowish area from the tip to the total leaf area. The dry biomass of the shoot was also determined after 18 and 28 days of growth in the soil pots.

Growth promotion assay by inoculation of *Oxalobacteraceae* isolates in the soil pots

To check whether *Oxalobacteraceae* can promote maize growth under nitrogen poor conditions, the *C2-Idf* and another lateral root defective mutants *lrt1* and *rum1* were inoculated by independent strains isolated from natural soils from Cologne, Germany[9] (50.96 N, 6.86 E) and Merelbeke, Belgium[57] (50.58 N, 3.46 E), respectively (Supplementary Dataset 15). Before inoculation of these 16 strains, we first mapped the 16S reads for rhizosphere samples of C2 and the *C2-Idf* mutant to the sequences of 16 *Oxalobacteraceae* strains (3 *Collimonas* strains, 1 *Duganella* strain, 1 *Herbaspirillum* strain, 2 *Janthinobacterium* strains, 4 *Massilia* strains, 2 *Pseudoduganella* strains and 3 strains with unknown genera) using HISAT2 (http://daehwankimlab.github.io/hisat2/) with default parameters. Before the inoculation experiment, the maize seeds were surface-sterilized. Briefly, seeds were washed 5 min with sterile water, 2 min with 70% (v/v) ethanol, 20 min with a bleach solution (29 ml sterile water, 15 ml NaClO, 12-13% (v/v) stock solution of 1 ml Tween 20), and finally 5 times for 15 min with sterile water. Seeds were then dried before pre-germination. The seeds were pre-germinated for 48 h then seedlings with similar primary root length (ca. 1-2 cm) were selected for inoculation. *Oxalobacteraceae* strains (6 strains from Belgian collections and 10 strains German collections) were cultured in R2A liquid medium overnight at 28 °C followed by centrifuged the culture at 1500 rcf for 10 min. Then the pellet was resuspended with 1 × PBS buffer and diluted until OD_{600} 0.02. For each round of inoculation, at least 10 seedlings were inoculated by shaking in a bacterial solution for 3 h and more than 6 seedlings were transferred to the sterilized natural Cologne soil with low nitrogen and grown in the phytochamber (16 h/8 h light/dark and 26 °C/18 °C). Specifically, we also performed the inoculation for *lrt1* mutants using the same four *Massilia* strains to understand their functions under the nitrogen-poor soil with sufficient supply of nitrogen. All pots were randomized on one tray for each biological replicate and each pot was watered with 20 ml sterilized dH_2O every day. For high nitrogen treatment, 20 ml nitrogen-rich nutrient solution (2 mM NH_4NO_3) was complemented to each pot with the same nitrogen-poor soil before potting and solution was supplied once a week. After four weeks of growth, plants were harvested and the total dry weight was determined. The lateral root density was calculated as the number of emerged lateral roots per unit length (cm) of the main root by hand. The effect of each strain was tested for two rounds of experiments.

Detection of indolic compounds production by *Oxalobacteraceae* strains

To check whether *Oxalobacteraceae* strains can produce indolic compounds, those strains were cultured in R2A medium with or without 0.1% tryptophan for 24 h at 28 °C. Analyses were performed on supernatant and bacterial cultures. Standard IAA curves were determined using 0, 0.5, 20, 50 and 100 µg/ml in R2A. The colorimetric assay was performed using Salkowski reagent[98], which consisted of 4.5 g of $FeCl_3$ and 22.3 ml of H_2SO_4 and 77.7 ml water. 1 ml of Salkowski reagent was mixed with 1 ml of the sample solution, and the mixture was left in the dark for 30 min at room temperature. The absorption spectra of a 200 µl mixture was determined at 530 nm in 96 well plates. Three technical replicates were performed for each sample.

DR5::GUS* staining of auxin induction by *Oxalobacteraceae* in *Arabidopsis

To validate whether *Oxalobacteraceae* strains can induce auxin production, *Oxalobacteracea* strains were cultured in R2A medium overnight at 28 °C. Bacterial cultures were centrifuged and bacterial cells were resuspended in 1 × PBS buffer. The concentration of the inoculums was adjusted to OD600 = 0.01. The *DR5::GUS* auxin responsive lines were used to study the auxin response of the bacterial inoculation in *Arabidopsis*. In brief, *DR5::GUS Arabidopsis* seeds were surface sterilized and vernalized for two days before sowing on ½ MS medium. The roots of 4-day-old seedlings were inoculated with 8 µl of the bacterial inoculum. GUS staining was performed 3 h and 3 days after inoculation. GUS signalling was checked under the light microscope (Leica) according to the manufacture instructions. The experiment was performed in three replicates on eight seedlings per replicate.

Data availability

All raw plant RNA sequencing data, rhizosphere bacterial 16S and fungal ITS and shotgun metagenomic sequencing data reported in this paper were deposited in the Sequence Read Archive (http://www.ncbi.nlm.nih.gov/sra) under accession number SRP263360. RNA sequencing reads were mapped to the maize reference genome sequence v4 (https://www.maizegdb.org/genome/genome_assembly/Zm-B73-REFERENCE-GRAMENE-4.0). The SSUrRNA database from SILVA database (release 128, 2016, https://www.arb-silva.de/) and UNITE database (v7.2, 2017, https://unite.ut.ee/) were used for analysing the bacterial 16S and fungal ITS sequences, respectively. The AgriGO (v2.0, 2017, http://systemsbiology.cau.edu.cn/agriGOv2/) and REVIGO databases (2017, http://revigo.irb.hr/) were used for functional GO analysis of maize genes. Protein-protein interaction networks of enriched gene modules were generated by STRING database (v10.5, https://version-10-5.string-db.org/). Functional annotation of shotgun metagenomic sequencing was performed using COG databases (Release clovr-1.0-RC9). We deposited customized scripts about association of gene modules with microbial taxonomic traits in the following GitHub repository: https://github.com/PengYuMaize/Yu2021NaturePlants. All statistical source data are provided with this paper.

Main figures

Figure 1. Interkingdom multi-omics demonstrates causal plant-microbial interactions in the rhizosphere during root development. a, Schematic illustration of plant-microbe interactions along the developmental zones and illustration of the separated root zones. Zone 1, the meristematic zone and the apical part of elongation zone; Zone 2, basal part of the elongation zone and apical part of differentiation zone with root hairs and lateral root primordia; Zone 3, the basal part of the differentiation zone with root hairs and emerged lateral roots. MZ, meristematic zone; EZ, elongation zone; DZ, differentiation zone. Dynamic patterns of exudation rate, microbial density, root nutrient uptake capacity and soil nutrient availability along the rhizosphere are modified from Marschner (2012)[3]. Principal component analysis (PCA) displaying the transcriptomic shift (**b**) and the dissimilarity of bacterial (**d**) and fungal (**e**) diversity along the root developmental zones ($p = 0.001$, permutational multivariate analysis of variance by ANOSIM). **c**, Network analysis of significantly enriched GO terms among the nine developmental zone-associated modules. The proportional distribution of GO terms is visualized by REVIGO and only the major host GO term representing the highest proportion is indicated by different colour codes corresponding to Supplemental Dataset 4. The whole panel of representative GO terms identified by TreeMap view of REVIGO (%) is provided in the Supplementary Dataset 4. The node size corresponds to the total number of interacted GO terms for each module. The thickness of the edges denotes the number of overlapped GO terms between each two modules. The solid and dotted edges indicate positive and negative relationships, respectively. Growth and defence related modules are highlighted with blue and red outlines, respectively. **f**, Covariance analysis highlighting direct associations between host root expressed genes and rhizosphere microbial OTUs (FDR corrected $p < 0.001$). **g**, Functional associations between gene-enriched modules and microbial orders. Growth and defence related modules are highlighted with blue and red outlines, respectively. The size of the circle corresponds to the sample size. The cumulative correlation is calculated as the sum of Pearson's correlations between modules and their corresponding microbial orders. *p* values, which were calculated using two-tailed Wilcoxon rank sum test, are indicating significance. The boxes span from the first to the third quartiles, the centre lines represent the median values and the whiskers show the data that lie within the 1.5 interquartile range of the lower and upper quartiles. The data points at the ends of the whiskers represent the outliers.

Figure 2. Host transcriptome and rhizosphere microbiome interactions affecting maize performance. a, Identification of phylogenetic and genotype specific gene modules by WGCNA network analyses. Each module is functionally annotated by gene ontology (GO) analysis and statistical test by Fisher´s exact test with Yekutieli adjustment (FDR corrected $p < 0.05$). Coloured dots and bars correspond to different inbred lines and their phylogenetic relationships in the field experiment (Supplementary Figure 1a). **b**, Correlation-based network between genotype-specific modules (nodes) and the bacterial taxa (triangles) at the phylum level. Pearson's correlation is calculated by relating the eigengene of each module with the relative abundance of each taxon using WGCNA "trait" function. Heat map indicates FDR corrected *p* values <0.05. The node size corresponds to the size of each module. The thickness and the colour of the edges denotes the strength and the significance of

correlations. The solid and dotted edges indicate positive and negative correlations, respectively. **c**, Genotype 787-specific module-taxa correlation and relative abundance (RA) at the family level. The plot shows bacterial families with ≥1% relative abundance. Average relative abundance values are indicated by circle size. Coloured circles denote Pearson's correlation coefficient (PCC) of each family with eigengene of module 5. **d**, Transcript abundance of module eigengene corresponding to genotype 787 in comparison to the other genotypes. *FNSI2*, *flavone synthase typeI2*. *n* = 9 biologically independent samples. Significances were indicated between inbred line 787 and other genotypes by exact *p* values (ANOVA, Tukey HSD). **e**, Concentrations of the two flavones apigenin and luteolin in root extracts or exudates. For root extracts and exudates, *n* = 4 and *n* = 5 biologically independent samples were collected, respectively. Data are the mean ± s.e.m. For each flavone type, *p* values were calculated using two-tailed unpaired t-tests according to the F-test results. **f**, Growth performance of 787 and LH93 grown in sterilized and unsterilized nitrogen-poor soil. *p* values were calculated using two-tailed unpaired t-tests according to the F-test results and were adjusted for each soil condition. **g**, Recovery of LH93 growth with 787-conditioned soil by rhizosphere transplantation. Significances were indicated among transplanted groups by exact *p* values (ANOVA, Tukey HSD). For **f** and **g**, *n* = 10 biologically independent samples over two independent experiments. DAT, days after transfer. For **d,** **f**, and **g**, the boxes span from the first to the third quartiles, the centre lines represent the median values and the whiskers show the data that lie within the 1.5 interquartile range of the lower and upper quartiles. The data points at the ends of the whiskers represent the outliers.

Figure 3. Changes in rhizosphere microbiota conditioned by plant-derived flavones promote maize growth and nitrogen uptake in nitrogen-poor soil. a, Simplified flavone biosynthesis pathway. The enzymes in the pathway are: ACC, acetyl-CoA carboxylase; CHI, chalcone isomerase; CHS, chalcone synthase; F3H, flavanone 3-hydroxylase; FLS, flavonol synthase; FNS, flavone synthase. Mutation of CHS in the *C2-Idf* mutant is highlighted in red. **b**, Nitrogen deficient phenotype in leaves of the maize mutant *C2-Idf* compared to wild-type C2 leaves. **c**, Growth performance of 3-week-old C2 wild-type and *C2-Idf* mutant plants grown in nitrogen-poor soil with and without prior sterilization. *n* = 10 biologically independent samples over two independent experiments. For each condition, *p* values were calculated using two-tailed unpaired t-tests according to the F-test results. The boxes span from the first to the third quartiles, the centre lines represent the median values and the whiskers show the data that lie within the 1.5 interquartile range of the lower and upper quartiles. The data points at the ends of the whiskers represent the outliers. **d**, Soil in which C2 plants were grown rescues the nitrogen deficient phenotype of *C2-Idf* mutants by rhizosphere transplantation. Each data point represents the mean nitrogen deficiency index (mean ± s.e.m.). *n* = 5 biologically independent samples. Different letters indicate significantly different groups (BH adjusted $p < 0.05$, Wilcoxon rank sum test). **e**, Representative leaf phenotype of C2 and its mutant *C2-Idf* after rhizosphere transplantation. **f**, Distinct bacterial diversity associated with C2 and its mutant rhizosphere microbiomes. **g**, Differences in the relative abundance of bacterial families associated with C2 and mutant *C2-Idf* rhizosphere microbiomes. *n* = 3 biologically independent samples. Significances are calculated by multiple test correction (FDR adjusted $*p < 0.05$, Welch's t-test). **h**, Effects of exogenously applied flavonoid types on the variations of bacterial diversity of the *C2-Idf* mutant rhizosphere. **i**, Effects of exogenously applied flavonoid types

on the family-level distribution (%) of the bacterial community of the *C2-Idf* mutant rhizosphere. *n* = 5 biologically independent samples. Different letters denote significance at $p < 0.05$ (ANOVA, Tukey HSD).

Figure 4. Growth performance of mutants with lateral root defects is associated with flavone-conditioned rhizosphere microbiota. a, Shoot growth performance of root mutants in nitrogen-poor soil. *n* = 25 biologically independent samples over three independent experiments. **b**, Shoot nitrogen concentration and accumulation of root mutants in nitrogen-poor soil. *n* = 6 biologically independent samples. **c**, Performance of lateral root defective mutants grown under in nitrogen-poor soil with and without subsequent sterilization. *n* = 10 biologically independent samples. For each genotype, *p* values were calculated using two-tailed unpaired *t*-tests according to the *F*-test results. **d**, Targeted metabolite profiling indicates that *lrt1* mutant produces and releases more flavone to the rhizosphere than the reference inbred line B73 and the mutant *rum1*. For root extracts and exudates, *n* = 4 and *n* = 5 biologically independent samples, respectively. Data are the mean ± s.e.m. Soil in which flavonoid enriched plants were grown is able to promote *lrt1* growth (**e**) and nitrogen acquisition (**f**) as demonstrated by rhizosphere transplantation. *n* = 5 biologically independent samples. Experimental schemes of the rhizosphere transplantation of *lrt1* and *rum1* with different genotypes containing different concentrations of flavones are highlighted. For **a**, **b**, **d**, **e** and **f**, significances were indicated among different groups by exact *p* values (ANOVA, Tukey HSD). For **a**, **b**, **c**, **e** and **f**, the boxes span from the first to the third quartiles, the centre lines represent the median values and the whiskers show the data that lie within the 1.5 interquartile range of the lower and upper quartiles. The data points at the ends of the whiskers represent the outliers.

Figure 5. Flavonoid-dependent *Oxalobacteraceae* promote plant growth and nitrogen acquisition by triggering developmental feedback on lateral root formation in nitrogen-poor soil. **a**, Shift of the rhizosphere bacterial α-diversity (Shannon's diversity index) along the developmental zones for each mutant and B73. *n* = 3 biologically independent samples. **b**, LEfSe cladogram indicating the phylogenetic distribution of bacterial lineages in the rhizosphere among different root mutants. Coloured circles show differentially abundant taxa and the colour is corresponding to the different root mutants in which the taxon displays the highest abundance. The six rings of the cladogram represent from inside to outside: domain, phylum, class, order, family, genus, and lineages with linear discriminant analysis (LDA) values >4 are displayed. Different letters of bar plot correspond to the bacterial taxa for class, order and family of the pie chart. **c**, Flavonoid-enriched plants grown soil is able to promote lateral root formation of *lrt1* by rhizosphere transplantation. A picture indicates more emerged lateral roots by rhizosphere transplantation of genotype 787. **d**, Correlation between lateral root density and shoot performance after inoculation with independent soil-derived *Oxalobacteraceae* isolates for *lrt1* mutant grown in nitrogen-poor soil. Scatter plots show combined data from two independent inoculation experiments with best fit (solid line) and 95% confidence interval (grey shade) for linear regression ($p < 2.2 \times 10^{-16}$; *n* = 10; Supplementary Figure 17). For **c** and **d**, *n* = 10 biologically independent samples over two independent experiments. For **a** and **c**, significances were indicated among different groups by exact *p* values (ANOVA, Tukey HSD). The boxes span from the first to the third quartiles, the centre

lines represent the median values and the whiskers show the data that lie within the 1.5 interquartile range of the lower and upper quartiles. The data points at the ends of the whiskers represent the outliers.

Figure 6. Proposed model for flavone-dependent, microbiota-mediated lateral root formation and plant performance. In nitrogen-poor soil, high content of flavone in root extracts and its exudates could cause a compositional shift of the rhizosphere microbiota by enrichment of *Oxalobacteraceae*, which indirectly boosts plant growth and nitrogen uptake by inducing lateral root formation in maize *lrt1* mutant.

Acknowledgements

We would like to thank P. Schulze-Lefert (Max Planck Institute for Plant Breeding Research, Cologne, Germany) for the generous donation of the bacterial strains and natural soil for pot experiments. We thank J. Birchler (University of Missouri, Columbia, USA), C. Gardener (United States Department of Agriculture, Ames, US), P. S. Schnable (Iowa State University, Ames, US), and T. Wang (Chinese Academy of Agricultural Sciences, Beijing, China) for germplasm contribution. We thank Seon-Woo Lee (Dong-A University, Busan, Republic of Korea) and Jihyun F Kim (Yonsei University, Seoul, Republic of Korea) for sharing methods for rhizosphere transplantation. We thank C. Gutjahr (Technical University of Munich, Munich, Germany), C. Knief (University of Bonn, Bonn, Germany) and B. Niu (Northeast Forest University of China, Harbin, China) for valuable suggestions on the experiments. We thank the student helpers from C. Zou´s group at China Agricultural University (Beijing, China) for the field sample harvest. We thank the technician Mrs. A. Glogau (University of Bonn, Bonn, Germany) for nitrogen determination. This work is supported by DFG grants HO2249/9-3, HO2249/12-1 to F.H. and YU272/1-1, Emmy Noether Programme (444755415) to P.Y., Germany's Excellence Strategy - EXC 2070 - PhenoRob grant 390732324 to G.S., Bundesministerium für Bildung und Forschung (BMBF) grant 031B195C to F.H. and DFG Priority Program (SPP2089) "Rhizosphere Spatiotemporal Organisation - a Key to Rhizosphere Functions" grant 403671039 to F.H. and P.Y. and 403670038 to B.S.R. S.G.'s research is supported by Research Foundation - Flanders - Strategic Basic Research (grant no. 151553). K.T.'s research is supported by the Huazhong Agricultural University Scientific & Technological Self-innovation Foundation, the Max Planck Society and DFG grant SPP2125. X.C.'s research is supported by The Changjiang Scholarship, Ministry of Education, China, State Cultivation Base of Eco-agriculture for Southwest Mountainous Land (Southwest University, Chongqing, China), and the National Maize Production System in China (grant no. CARS-02-15).

References

1. Brundrett, M. C. Coevolution of roots and mycorrhizas of land plants. *New Phytol.* **154**, 275-304 (2002).
2. Kenrick, P. & Strullu-Derrien, C. The origin and early evolution of roots. *Plant Physiol.* **166**, 570-580 (2014).
3. Marschner P. 2012. Rhizosphere biology. In: Marschner P., ed. *Marschner's mineral nutrition of higher plants*, 3rd edn. San Diego: Academic Press, 369-388.
4. Berendsen, R. L., Pieterse, C. M. & Bakker, P. A. The rhizosphere microbiome and plant health. *Trends Plant Sci.* **17**, 478-486 (2012).
5. Mendes, R., Garbeva, P. & Raaijmakers, J. M. The rhizosphere microbiome: significance of plant beneficial, plant pathogenic, and human pathogenic microorganisms. *FEMS Microbiol. Rev.* **37**, 634-663 (2013).
6. Haney, C. H., Samuel, B. S., Bush, J. & Ausubel, F. M. Associations with rhizosphere bacteria can confer an adaptive advantage to plants. *Nat. Plants*. **1**, 15051 (2015).
7. Kwak, M. J. et al. Rhizosphere microbiome structure alters to enable wilt resistance in tomato. *Nat. Biotechnol.* **36**, 1100 (2018).
8. Lu, T. et al. Rhizosphere microorganisms can influence the timing of plant flowering. *Microbiome* **6**, 231 (2018).
9. Bulgarelli, D. et al. Revealing structure and assembly cues for *Arabidopsis* root-inhabiting bacterial microbiota. *Nature* **488**, 91 (2012).
10. Lundberg, D. S. et al. Defining the core *Arabidopsis thaliana* root microbiome. *Nature* **488**, 86 (2012).
11. Schreiter, S. et al. Effect of the soil type on the microbiome in the rhizosphere of field-grown lettuce. *Front. Microbiol*. **5**, 144 (2014).
12. Veach, A. M. et al. Rhizosphere microbiomes diverge among *Populus trichocarpa* plant-host genotypes and chemotypes, but it depends on soil origin. *Microbiome* **7**, 76 (2019).
13. Turner, T. R., James, E. K. & Poole, P. S. The plant microbiome. *Genome Biol*. **14**, 209 (2013).
14. Ofek-Lalzar, M. et al. Niche and host-associated functional signatures of the root surface microbiome. *Nat. Commun.* **5**, 4950 (2014).
15. Fitzpatrick, C. R. et al. Assembly and ecological function of the root microbiome across angiosperm plant species. *Proc. Natl Acad. Sci. USA* **115**, E1157-E1165 (2018).
16. Gruber, B., Giehl, R., Friedel, S. & von Wirén N. Plasticity of the *Arabidopsis* root system under nutrient deficiencies. *Plant Physiol.* **163**, 161-179 (2013).
17. Garrido-Oter, R. et al. Modular traits of the rhizobiales root microbiota and their evolutionary relationship with symbiotic rhizobia. *Cell Host Microbe* **24**, 155-167 (2018).
18. Verbon, E. H. & Liberman, L. M. Beneficial microbes affect endogenous mechanisms controlling root development. *Trends Plant Sci.* **21**, 218-229 (2016).
19. Hochholdinger, F., Yu, P. & Marcon, C. Genetic control of root system development in maize. *Trends Plant Sci.* **23**, 79-88 (2018).
20. Hake, S. & Ross-Ibarra, J. The natural history of model organisms: genetic, evolutionary and plant breeding insights from the domestication of maize. *Elife* **4**, e05861 (2015).
21. Yu, P., Gutjahr, C., Li, C. & Hochholdinger, F. Genetic control of lateral root formation in cereals. Trends Plant Sci. **21**, 951-961 (2016a).
22. Tai, H. et al. Transcriptomic and anatomical complexity of primary, seminal, and crown roots highlight root type-specific functional diversity in maize (*Zea mays* L.). *J. Exp. Bot.* **67**, 1123-1135 (2015).
23. Yu, P., Eggert, K., von Wirén, N., Li, C. & Hochholdinger, F. Cell type-specific gene expression analyses by RNA sequencing reveal local high nitrate-triggered lateral root initiation in shoot-borne roots of maize by modulating auxin-related cell cycle regulation. *Plant Physiol.* **169**, 690-704 (2015).
24. Yu, P. et al. Root type-specific reprogramming of maize pericycle transcriptomes by local high nitrate results in disparate lateral root branching patterns. *Plant Physiol.* **170**, 1783-1798 (2016b).

25. Szoboszlay, M. et al. Comparison of root system architecture and rhizosphere microbial communities of Balsas teosinte and domesticated corn cultivars. *Soil Biol. Biochem.* **80**, 34-44 (2015).
26. Gutjahr, C. et al. Transcriptome diversity among rice root types during asymbiosis and interaction with arbuscular mycorrhizal fungi. *Proc. Natl Acad. Sci. USA* **112**, 6754-6759 (2015).
27. Yu, P. et al. Root type and soil phosphate determine the taxonomic landscape of colonizing fungi and the transcriptome of field-grown maize roots. *New Phytol.* **217**, 1240-1253 (2018).
28. Cotton, T. A. et al. Metabolic regulation of the maize rhizobiome by benzoxazinoids. *ISME J.* **13**, 1647-1658 (2019).
29. Zhang, J. et al. *NRT1. 1B* is associated with root microbiota composition and nitrogen use in field-grown rice. *Nat. Biotechnol.* **37**, 676-684 (2019).
30. Peiffer, J. A. et al. Diversity and heritability of the maize rhizosphere microbiome under field conditions. *Proc. Natl Acad. Sci. USA* **110**, 6548-6553 (2013).
31. Walters, W. A. et al. Large-scale replicated field study of maize rhizosphere identifies heritable microbes. *Proc. Natl Acad. Sci. USA* **115**, 7368-7373 (2018).
32. Cesco, S., Neumann, G., Tomasi, N., Pinton, R. & Weisskopf, L. Release of plant-borne flavonoids into the rhizosphere and their role in plant nutrition. *Plant Soil **329***, 1-25 (2010).
33. Hu, L. et al. Root exudate metabolites drive plant-soil feedbacks on growth and defense by shaping the rhizosphere microbiota. *Nat. Commun.* **9**, 2738 (2018).
34. Kudjordjie, E. N., Sapkota, R., Steffensen, S. K., Fomsgaard, I. S. & Nicolaisen, M. Maize synthesized benzoxazinoids affect the host associated microbiome. *Microbiome* **7**, 59 (2019).
35. Hassan, S. & Mathesius, U. The role of flavonoids in root-rhizosphere signalling: opportunities and challenges for improving plant-microbe interactions. *J. Exp. Bot.* **63**, 3429-3444 (2012).
36. Mierziak, J., Kostyn, K. & Kulma, A. Flavonoids as important molecules of plant interactions with the environment. *Molecules* **19**, 16240-16265 (2014).
37. Ferreyra, M. L. F. et al. The identification of maize and *Arabidopsis* type I flavone synthases links flavones with hormones and biotic interactions. *Plant Physiol.* **169**, 1090-1107 (2015).
38. Eloy, N. B. et al. Silencing CHALCONE SYNTHAS E in maize impedes the incorporation of tricin into lignin and increases lignin content. *Plant Physiol.* **173**, 998-1016 (2017).
39. Righini, S., Rodriguez, E.J., Berosich, C., Grotewold, E., Casati, P. & Falcone Ferreyra, M.L. Apigenin produced by maize flavone synthase I and II protects plants against UV-B-induced damage. *Plant Cell Environ*. **42**, 495-508 (2019).
40. Wasson, A. P., Pellerone, F. I. & Mathesius, U. Silencing the flavonoid pathway in *Medicago truncatula* inhibits root nodule formation and prevents auxin transport regulation by rhizobia. *Plant Cell* **18**, 1617-1629 (2006).
41. Subramanian, S., Stacey, G. & Yu, O. Distinct, crucial roles of flavonoids during legume nodulation. *Trends Plant Sci.* **12**, 282-285 (2007).
42. Oldroyd, G. E. & Leyser, O. A plant's diet, surviving in a variable nutrient environment. *Science* **368**, eaba0196 (2020).
43. Zhang, J., Subramanian, S., Stacey, G., & Yu, O. Flavones and flavonols play distinct critical roles during nodulation of *Medicago truncatula* by *Sinorhizobium meliloti*. *Plant J.* **57**, 171-183 (2009).
44. de Vries, F. T., Griffiths, R. I., Knight, C. G., Nicolitch, O. & Williams, A. Harnessing rhizosphere microbiomes for drought-resilient crop production. *Science* **368**, 270-274 (2020).
45. Barberon, M. The endodermis as a checkpoint for nutrients. *New Phytol.* **213**, 1604-1610 (2017).
46. Duan, F., Giehl, R. F. H., Geldner, N., Salt, D. E. & von Wirén, N. Root zone-specific localization of AMTs determines ammonium transport pathways and nitrogen allocation to shoots. *PLoS Biol.* **16**, e2006024 (2018).
47. Giehl, R. F. & von Wirén, N. Root nutrient foraging. *Plant Physiol.* **166**, 509-517 (2014).
48. Jia, Z., Giehl, R. F. H., Meyer, R. C., Altmann, T. & von Wirén, N. Natural variation of BSK3 tunes brassinosteroid signaling to regulate root foraging under low nitrogen. *Nat. Commun.* **10**, 2378 (2019).
49. Postma, J. A., Dathe, A. & Lynch, J. P. The optimal lateral root branching density for maize depends on nitrogen and phosphorus availability. *Plant Physiol.* **166**, 590-602 (2014).

50. Zhan, A. & Lynch, J. P. Reduced frequency of lateral root branching improves N capture from low-N soils in maize. *J. Exp. Bot.* **66**, 2055-2065 (2015).
51. Badri, D. V. & Vivanco, J. M. Regulation and function of root exudates. *Plant Cell Environ.* **32**, 666-681 (2009).
52. Sasse, J., Martinoia, E. & Northen, T. Feed your friends: do plant exudates shape the root microbiome? *Trends Plant Sci.* **23**, 25-41 (2018).
53. Stringlis, I. A. et al. MYB72-dependent coumarin exudation shapes root microbiome assembly to promote plant health. *Proc. Natl Acad. Sci. USA* **115**, E5213-E5222 (2018).
54. Voges, M. J., Bai, Y., Schulze-Lefert, P. & Sattely, E. S. Plant-derived coumarins shape the composition of an *Arabidopsis* synthetic root microbiome. *Proc. Natl Acad. Sci. USA* **116**, 12558-12565 (2019).
55. Lebeis, S. L. et al. Salicylic acid modulates colonization of the root microbiome by specific bacterial taxa. *Science* **349**, 860-864 (2015).
56. Bulgarelli, D. et al. Structure and function of the bacterial root microbiota in wild and domesticated barley. *Cell Host Microbe* **17**, 392-403 (2015).
57. Beirinckx, S. et al. Tapping into the maize root microbiome to identify bacteria that promote growth under chilling conditions. *Microbiome* **8**, 54 (2020).
58. Stelpflug, S. C. et al. An expanded maize gene expression atlas based on RNA sequencing and its use to explore root development. *Plant Genome* **9**, 1-15 (2016).
59. Ofek, M., Hadar, Y. & Minz, D. Ecology of root colonizing *Massilia* (*Oxalobacteraceae*). *PloS One* **7**, p.e40117 (2012).
60. Gutiérrez-Luna, F. M. et al. Plant growth-promoting rhizobacteria modulate root-system architecture in *Arabidopsis thaliana* through volatile organic compound emission. *Symbiosis* **51**, 75-83 (2010).
61. Poitout, A. et al. Local signalling pathways regulate the *Arabidopsis* root developmental response to *Mesorhizobium loti* inoculation. *J. Exp. Bot.* **68**, 1199-1211 (2017).
62. López-Bucio, J. et al. *Bacillus megaterium* rhizobacteria promote growth and alter root-system architecture through an auxin- and ethylene-independent signaling mechanism in *Arabidopsis thaliana*. *Mol. Plant-Microbe Interact.* **20**, 207-217 (2007).
63. Finkel, O. M. et al. A single bacterial genus maintains root development in a complex microbiome. *Nature* **587**, 103-108 (2020).
64. Schiessl, K. et al. NODULE INCEPTION recruits the lateral root developmental program for symbiotic nodule organogenesis in *Medicago truncatula*. *Curr. Biol.* **29**, 3657-3668 (2019).
65. Soyano, T., Shimoda, Y., Kawaguchi, M. & Hayashi, M. A shared gene drives lateral root development and root nodule symbiosis pathways in *Lotus*. *Science* **366**, 1021-1023 (2019).
66. Zhu, F. et al. A CEP peptide receptor-like kinase regulates auxin biosynthesis and ethylene signaling to coordinate root growth and symbiotic nodulation in *Medicago truncatula*. *Plant Cell* doi:10.1105/tpc.19.00428 (2020).
67. Romay, M. C.et al. Comprehensive genotyping of the USA national maize inbred seed bank. *Genome Biol.* **14**, R55 (2013).
68. Della Vedova, C. B. et al. The dominant inhibitory chalcone synthase allele C2-Idf (inhibitor diffuse) from *Zea mays* (L.) acts via an endogenous RNA silencing mechanism. *Genetics* **170**, 1989-2002 (2005).
69. Bertin, P. & Gallais, A. Genetic variation for nitrogen use efficiency in a set of recombinant maize inbred lines. I. Agrophysiological results. *Maydica* **45**, 53-66 (2000).
70. Nelson, D. W. & Sommers, L. E. Determination of total nitrogen in plant material. *Agron. J.* **65**, 109-112 (1973).
71. Edwards, J. et al. Structure, variation, and assembly of the root-associated microbiomes of rice. *Proc. Natl Acad. Sci. USA* **112**, E911-E920 (2015).
72. Smyth, G. K. Linear models and empirical Bayes methods for assessing differential expression in microarray experiments. *Stat. Appl. Genet. Mol. Biol.* **3**, Article 3 (2004).
73. Benjamini, Y. & Hochberg, Y. Controlling the false discovery rate: a practical and powerful approach to multiple testing. *J. R. Stat. Soc. B*. **57**, 289-300 (1995).
74. Tian, T. et al. agriGO v2. 0: a GO analysis toolkit for the agricultural community, 2017 update. *Nucleic Acids Res.* **45**, W122-W129 (2017).

75. Caporaso, J. G. et al. Global patterns of 16S rRNA diversity at a depth of millions of sequences per sample. *Proc. Natl Acad. Sci. USA* **108**, 4516-4522 (2011).
76. Magoč, T. & Salzberg, S. L. FLASH: fast length adjustment of short reads to improve genome assemblies. *Bioinformatics* **27**, 2957-2963 (2011).
77. Caporaso, J. G. et al. QIIME allows analysis of high-throughput community sequencing data. *Nat. Methods.* **7**, 335 (2010).
78. Bokulich, N. A. et al. Quality-filtering vastly improves diversity estimates from Illumina amplicon sequencing. *Nat. Methods* **10**, 57 (2013).
79. Edgar, R. C., Haas, B. J., Clemente, J. C., Quince, C. & Knight, R. UCHIME improves sensitivity and speed of chimera detection. *Bioinformatics* **27**, 2194-2200 (2011).
80. Haas, B. J. et al. Chimeric 16S rRNA sequence formation and detection in Sanger and 454-pyrosequenced PCR amplicons. *Genome Res.* **21**, 494-504 (2011).
81. Edgar, R. C. UPARSE: highly accurate OTU sequences from microbial amplicon reads. *Nat. Methods.* **10**, 996 (2013).
82. Wang, Q., Garrity, G. M., Tiedje, J. M. & Cole, J. R. Naive Bayesian classifier for rapid assignment of rRNA sequences into the new bacterial taxonomy. *Appl. Environ. Microb.* **73**, 5261-5267 (2007).
83. Quast, C. et al. The SILVA ribosomal RNA gene database project: improved data processing and web-based tools. *Nucleic Acids Res*. **41**, D590-D596 (2013).
84. Edgar, R. C. MUSCLE: multiple sequence alignment with high accuracy and high throughput. *Nucleic Acids Res.* **32**, 1792-1797 (2004).
85. Kõljalg, U. et al. Towards a unified paradigm for sequence-based identification of fungi. *Mol. Ecol*. **22**, 5271-5277 (2013).
86. Lê, S., Josse, J. & Husson, F. FactoMineR: an R package for multivariate analysis. *J. Stat. Softw*. **25**, 1-18 (2008).
87. Segata, N. & Huttenhower, C. Toward an efficient method of identifying core genes for evolutionary and functional microbial phylogenies. *PLoS One* **6**, e24704 (2011).
88. Durán, P. et al. Microbial interkingdom interactions in roots promote *Arabidopsis* survival. *Cell* **175**, 973-983 (2018).
89. Faust, K. & Raes, J. CoNet app: inference of biological association networks using Cytoscape. *F1000Res* **5**, 1519 (2016).
90. Shannon, P. et al. Cytoscape: a software environment for integrated models of biomolecular interaction networks. *Genome Res.***13**, 2498-2504 (2003).
91. Friedman, J. & Alm, E. J. Inferring correlation networks from genomic survey data. *PLoS. Comput. Biol*. **8**, e1002687 (2012).
92. Wang, Q., Wang, K., Wu, W., Giannoulatou, E., Ho, J. W. & Li, L. Host and microbiome multi-omics integration: applications and methodologies. *Biophys. Rev.* **11**, 55-65 (2019).
93. Langfelder, P. & Horvath, S. WGCNA: an R package for weighted correlation network analysis. *BMC Bioinformatics* **9**, 559 (2008).
94. Zhang, B. & Horvath, S. A general framework for weighted gene co-expression network analysis. *Stat. Appl. Genet. Mol.* **4** (2005).
95. Supek, F., Bošnjak, M., Škunca, N. & Šmuc, T. REVIGO summarizes and visualizes long lists of gene ontology terms. *PLoS One* **6**, e21800 (2011).
96. Tatusov, R. L. et al. The COG database: an updated version includes eukaryotes. *BMC Bioinformatics* **4**, 1-14 (2003).
97. Stiehl-Braun, P. A., Hartmann, A. A., Kandeler, E., Buchmann, N. I. N. A. & Niklaus, P. A. Interactive effects of drought and N fertilization on the spatial distribution of methane assimilation in grassland soils. *Global Change Biol*. **17**, 2629-2639 (2011).
98. Glickmann, E. & Dessaux, Y. A critical examination of the specificity of the salkowski reagent for indolic compounds produced by phytopathogenic bacteria. *Appl. Environ. Microbiol.* **61**, 793-796 (1995).

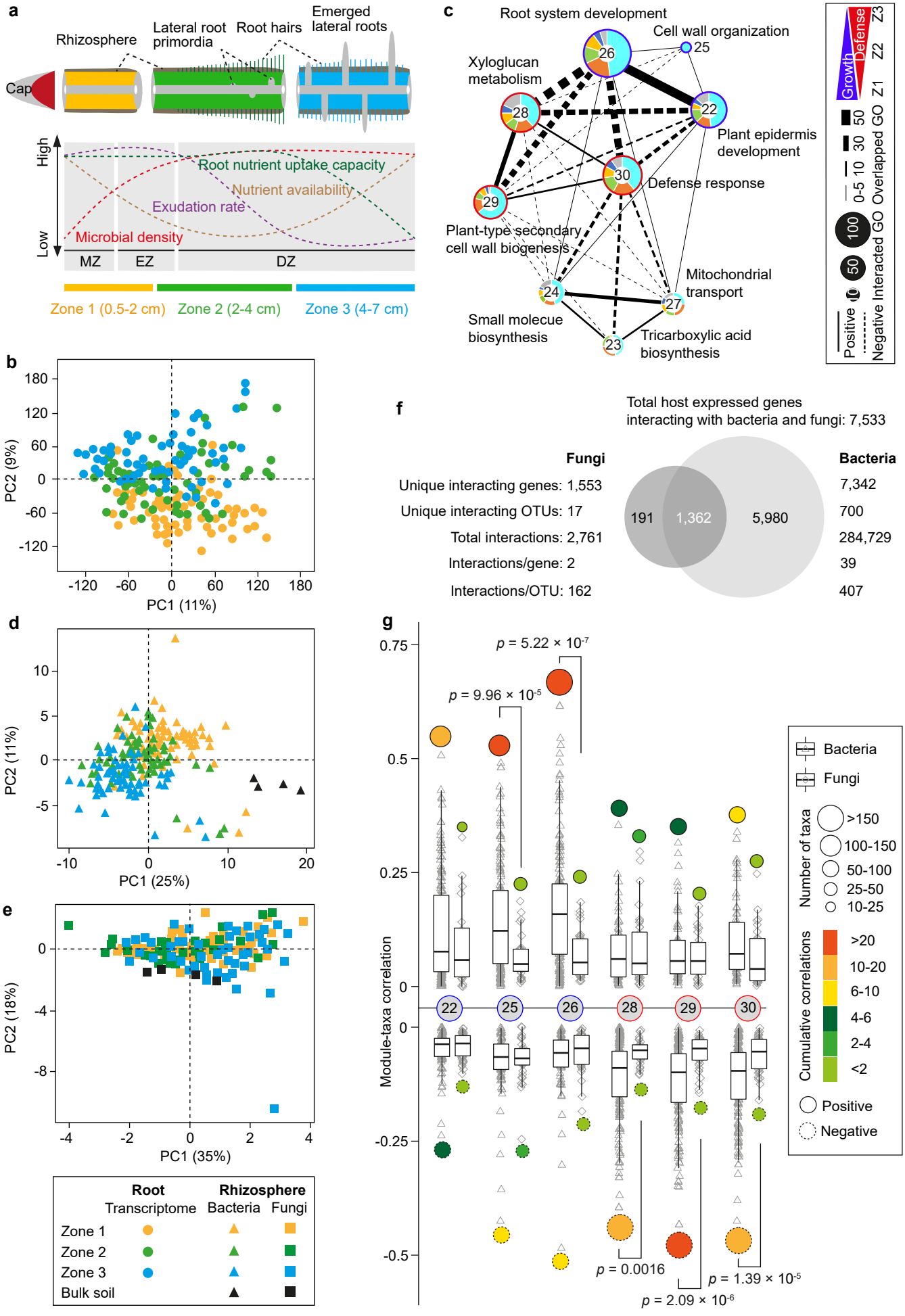
a
Rhizosphere
Lateral root primordia
Root hairs
Emerged lateral roots
Cap
High
Low
Root nutrient uptake capacity
Nutrient availability
Exudation rate
Microbial density
MZ
EZ
DZ
Zone 1 (0.5-2 cm)
Zone 2 (2-4 cm)
Zone 3 (4-7 cm)
b
PC2 (9%)
PC1 (11%)
c
Root system development
Cell wall organization
Xyloglucan metabolism
Plant epidermis development
Defense response
Plant-type secondary cell wall biogenesis
Mitochondrial transport
Small molecue biosynthesis
Tricarboxylic acid biosynthesis
Growth
Defense
Z3
Z2
Z1
Overlapped GO
Interacted GO
Positive
Negative
d
PC2 (11%)
PC1 (25%)
e
PC2 (18%)
PC1 (35%)
Root
Transcriptome
Rhizosphere
Bacteria
Fungi
Zone 1
Zone 2
Zone 3
Bulk soil
f
Total host expressed genes interacting with bacteria and fungi: 7,533
Fungi
Bacteria
Unique interacting genes: 1,553
Unique interacting OTUs: 17
Total interactions: 2,761
Interactions/gene: 2
Interactions/OTU: 162
191
1,362
5,980
7,342
700
284,729
39
407
g
p = 5.22 × 10-7
p = 9.96 × 10-5
Module-taxa correlation
p = 0.0016
p = 1.39 × 10-5
p = 2.09 × 10-6
Bacteria
Fungi
Number of taxa
>150
100-150
50-100
25-50
10-25
Cumulative correlations
>20
10-20
6-10
4-6
2-4
<2
Positive
Negative

Figure 1

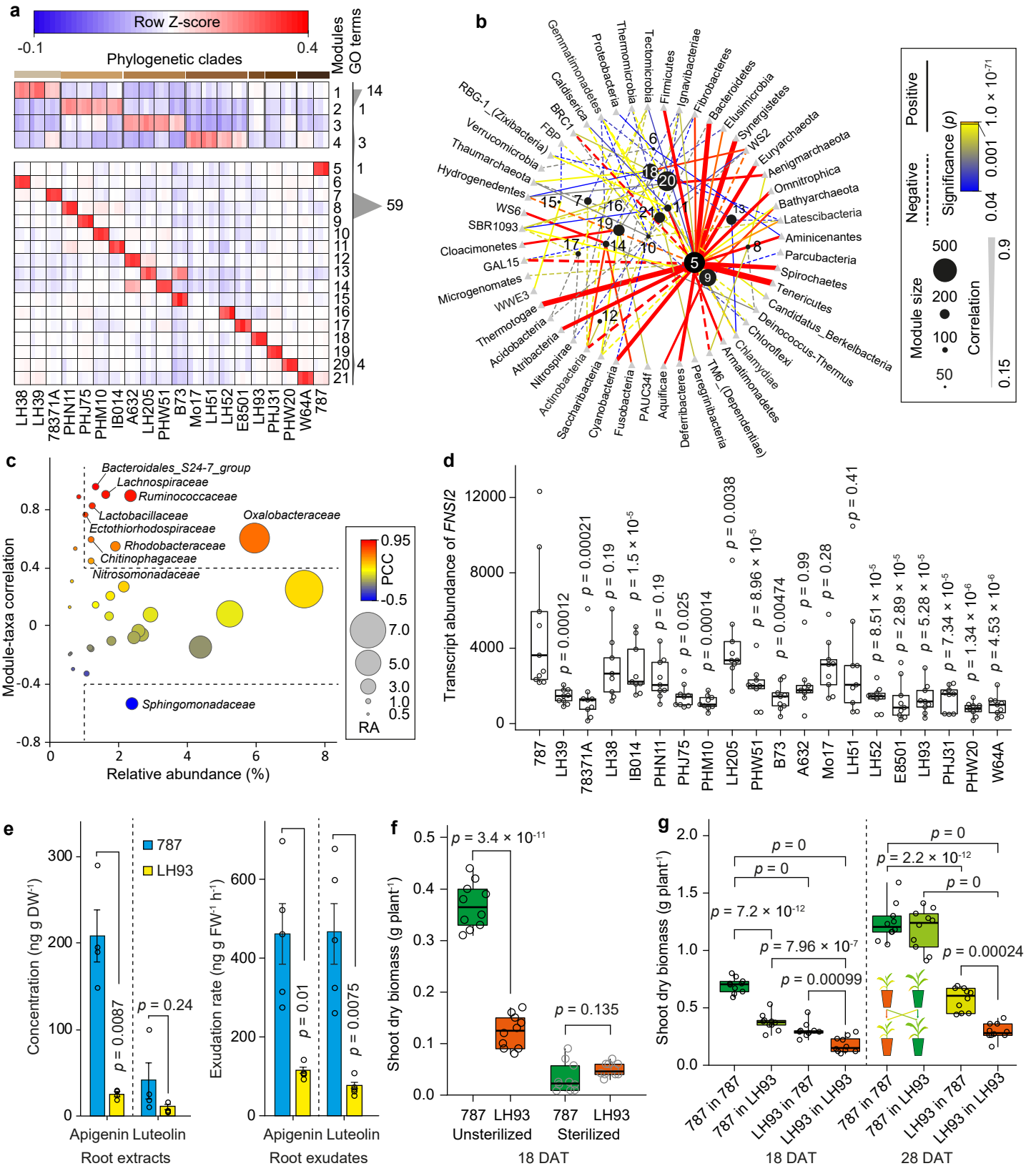
a
Row Z-score
-0.1
0.4
Phylogenetic clades
Modules
GO terms
14
1
3
1
59
4
LH38 LH39 78371A PHN11 PHJ75 PHM10 IB014 A632 LH205 PHW51 B73 Mo17 LH51 LH52 E8501 LH93 PHJ31 PHW20 W64A 787
b
Gemmatimonadetes
Proteobacteria
Thermomicrobia
Tectomicrobia
Firmicutes
Ignavibacteriae
Fibrobacteres
Bacteroidetes
Elusimicrobia
Synergistetes
WS2
Euryarchaeota
Aenigmarchaeota
Omnitrophica
Bathyarchaeota
Latescibacteria
Aminicenantes
Parcubacteria
Spirochaetes
Tenericutes
Candidatus_Berkelbacteria
Deinococcus-Thermus
Chloroflexi
Chlamydiae
Armatimonadetes
TM6_(Dependentiae)
Peregrinibacteria
Deferribacteres
Aquificae
PAUC34f
Fusobacteria
Cyanobacteria
Saccharibacteria
Actinobacteria
Nitrospirae
Atribacteria
Acidobacteria
Thermotogae
WWE3
Microgenomates
GAL15
Cloacimonetes
SBR1093
WS6
Hydrogenedentes
Thaumarchaeota
Verrucomicrobia
FBP
BRC1
Caldiserica
RBG-1_(Zixibacteria)
Positive
Negative
Significance (p)
1.0 × 10-71
0.001
0.04
Module size
500
200
100
50
Correlation
0.9
0.15
c
Bacteroidales_S24-7_group
Lachnospiraceae
Ruminococcaceae
Lactobacillaceae
Oxalobacteraceae
Ectothiorhodospiraceae
Rhodobacteraceae
Chitinophagaceae
Nitrosomonadaceae
Sphingomonadaceae
Module-taxa correlation
Relative abundance (%)
PCC
0.95
-0.5
7.0
5.0
3.0
1.0
0.5
RA
d
Transcript abundance of FNSI2
p = 0.00012
p = 0.00021
p = 0.19
p = 1.5 × 10-5
p = 0.19
p = 0.025
p = 0.00014
p = 0.0038
p = 8.96 × 10-5
p = 0.00474
p = 0.99
p = 0.28
p = 0.41
p = 8.51 × 10-5
p = 2.89 × 10-5
p = 5.28 × 10-5
p = 7.34 × 10-5
p = 1.34 × 10-6
p = 4.53 × 10-6
787 LH39 78371A LH38 IB014 PHN11 PHJ75 PHM10 LH205 PHW51 B73 A632 Mo17 LH51 LH52 E8501 LH93 PHJ31 PHW20 W64A
e
787
LH93
Concentration (ng g DW-1)
p = 0.0087
p = 0.24
Exudation rate (ng g FW-1 h-1)
p = 0.01
p = 0.0075
Apigenin Luteolin
Root extracts
Apigenin Luteolin
Root exudates
f
p = 3.4 × 10-11
p = 0.135
Shoot dry biomass (g plant-1)
787 LH93
Unsterilized
787 LH93
Sterilized
18 DAT
g
p = 0
p = 0
p = 7.2 × 10-12
p = 7.96 × 10-7
p = 0.00099
p = 0
p = 2.2 × 10-12
p = 0
p = 0.00024
Shoot dry biomass (g plant-1)
787 in 787
787 in LH93
LH93 in 787
LH93 in LH93
18 DAT
787 in 787
787 in LH93
LH93 in 787
LH93 in LH93
28 DAT

Figure 2

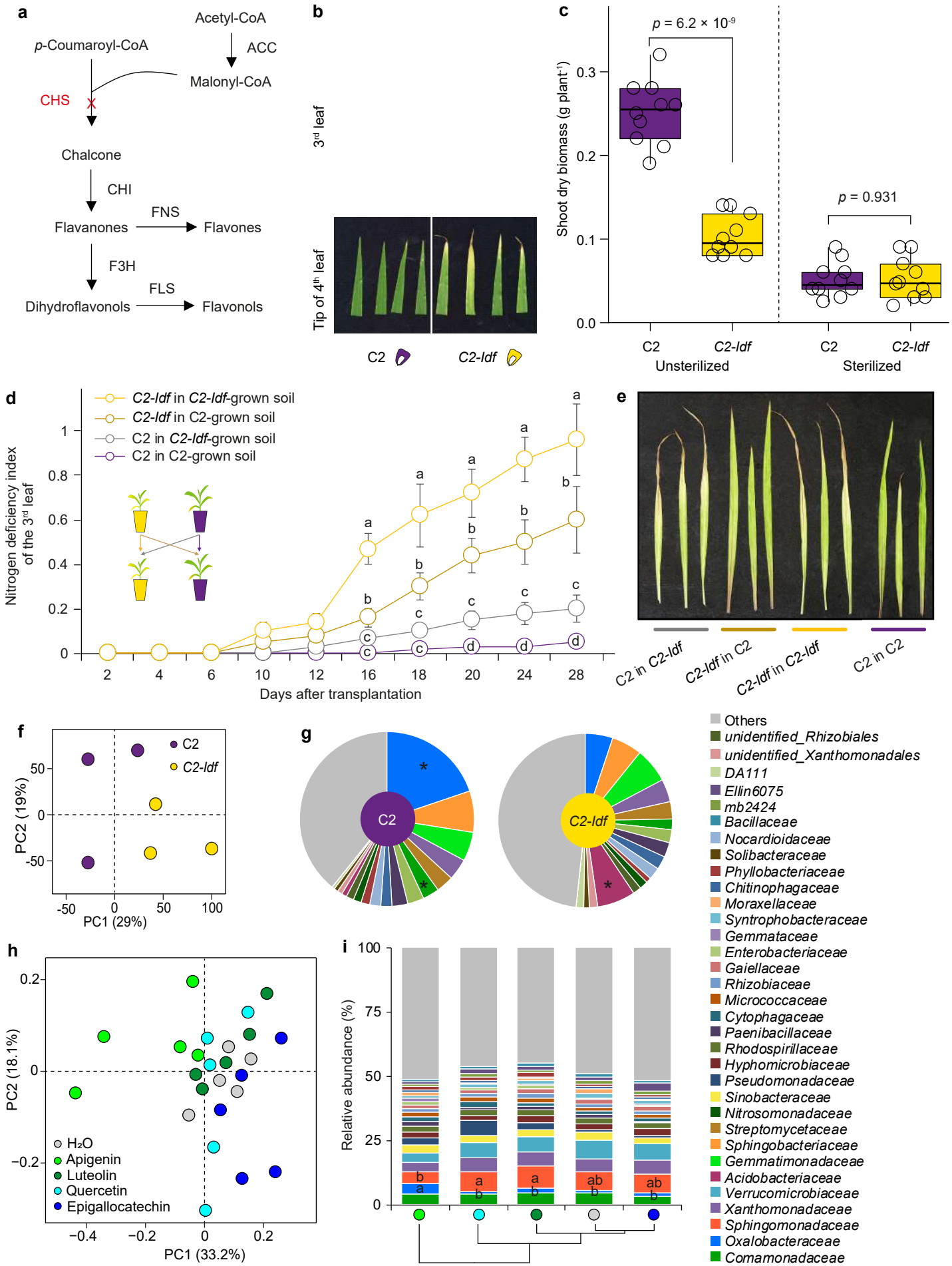
a
Acetyl-CoA
ACC
p-Coumaroyl-CoA
Malonyl-CoA
CHS
Chalcone
CHI
Flavanones
FNS
Flavones
F3H
Dihydroflavonols
FLS
Flavonols
b
3rd leaf
Tip of 4th leaf
C2
C2-Idf
c
p = 6.2 × 10-9
p = 0.931
Shoot dry biomass (g plant-1)
C2
C2-Idf
Unsterilized
Sterilized
d
C2-Idf in C2-Idf-grown soil
C2-Idf in C2-grown soil
C2 in C2-Idf-grown soil
C2 in C2-grown soil
Nitrogen deficiency index of the 3rd leaf
Days after transplantation
e
C2 in C2-Idf
C2-Idf in C2
C2-Idf in C2-Idf
C2 in C2
f
C2
C2-Idf
PC2 (19%)
PC1 (29%)
g
C2
C2-Idf
Others
unidentified_Rhizobiales
unidentified_Xanthomonadales
DA111
Ellin6075
mb2424
Bacillaceae
Nocardioidaceae
Solibacteraceae
Phyllobacteriaceae
Chitinophagaceae
Moraxellaceae
Syntrophobacteraceae
Gemmataceae
Enterobacteriaceae
Gaiellaceae
Rhizobiaceae
Micrococcaceae
Cytophagaceae
Paenibacillaceae
Rhodospirillaceae
Hyphomicrobiaceae
Pseudomonadaceae
Sinobacteraceae
Nitrosomonadaceae
Streptomycetaceae
Sphingobacteriaceae
Gemmatimonadaceae
Acidobacteriaceae
Verrucomicrobiaceae
Xanthomonadaceae
Sphingomonadaceae
Oxalobacteraceae
Comamonadaceae
h
H2O
Apigenin
Luteolin
Quercetin
Epigallocatechin
PC2 (18.1%)
PC1 (33.2%)
i
Relative abundance (%)

Figure 3

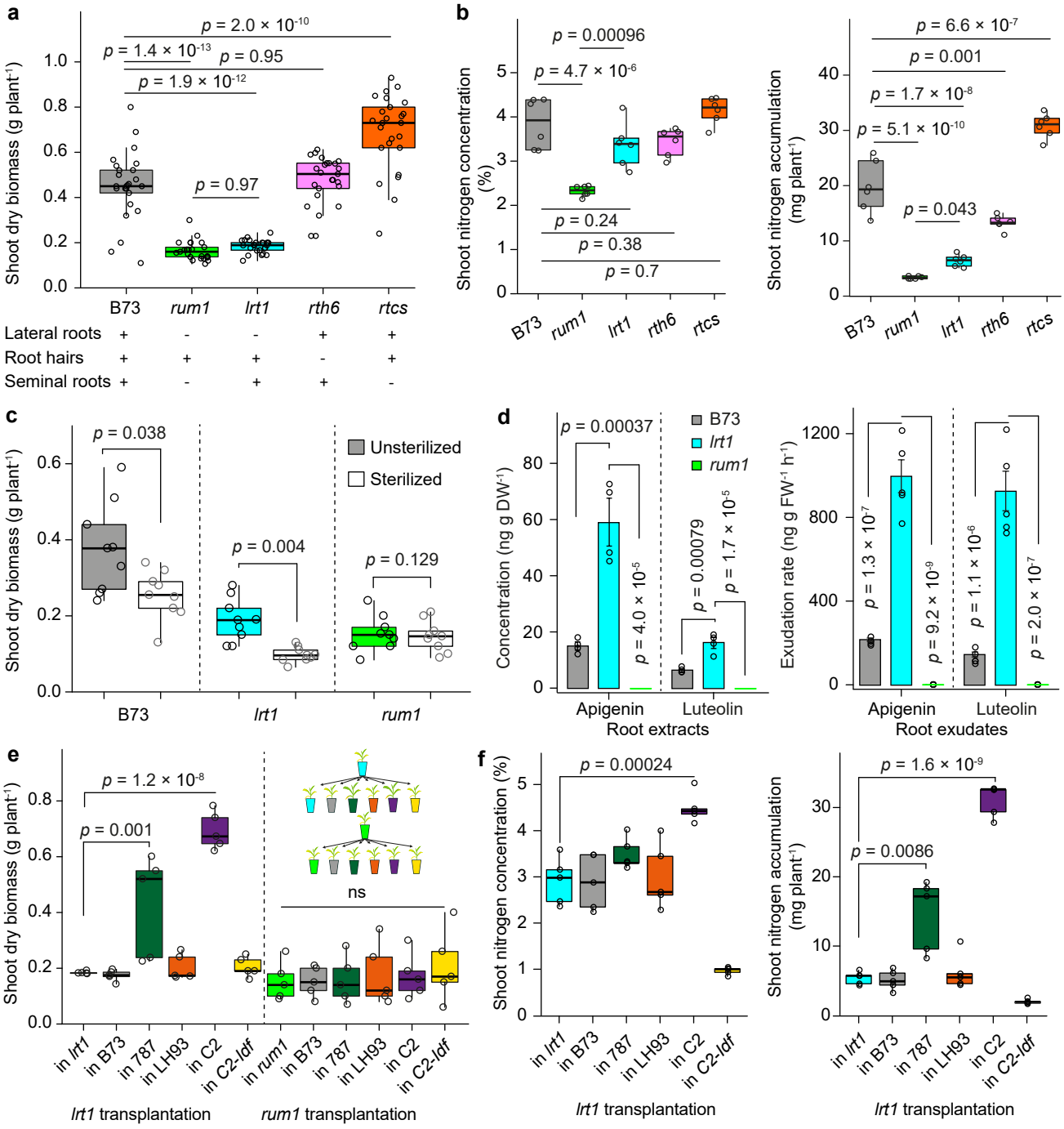
a
Shoot dry biomass (g plant-1)
p = 2.0 × 10-10
p = 1.4 × 10-13
p = 0.95
p = 1.9 × 10-12
p = 0.97
B73
rum1
lrt1
rth6
rtcs
Lateral roots + - - + +
Root hairs + + + - +
Seminal roots + - + + -
b
Shoot nitrogen concentration (%)
p = 0.00096
p = 4.7 × 10-6
p = 0.24
p = 0.38
p = 0.7
Shoot nitrogen accumulation (mg plant-1)
p = 6.6 × 10-7
p = 0.001
p = 1.7 × 10-8
p = 5.1 × 10-10
p = 0.043
c
Shoot dry biomass (g plant-1)
p = 0.038
p = 0.004
p = 0.129
Unsterilized
Sterilized
B73
lrt1
rum1
d
Concentration (ng g DW-1)
p = 0.00037
p = 4.0 × 10-5
p = 0.00079
p = 1.7 × 10-5
B73
lrt1
rum1
Apigenin
Luteolin
Root extracts
Exudation rate (ng g FW-1 h-1)
p = 1.3 × 10-7
p = 9.2 × 10-9
p = 1.1 × 10-6
p = 2.0 × 10-7
Root exudates
e
Shoot dry biomass (g plant-1)
p = 1.2 × 10-8
p = 0.001
ns
in lrt1
in B73
in 787
in LH93
in C2
in C2-ldf
in rum1
lrt1 transplantation
rum1 transplantation
f
Shoot nitrogen concentration (%)
p = 0.00024
Shoot nitrogen accumulation (mg plant-1)
p = 1.6 × 10-9
p = 0.0086
lrt1 transplantation

Figure 4

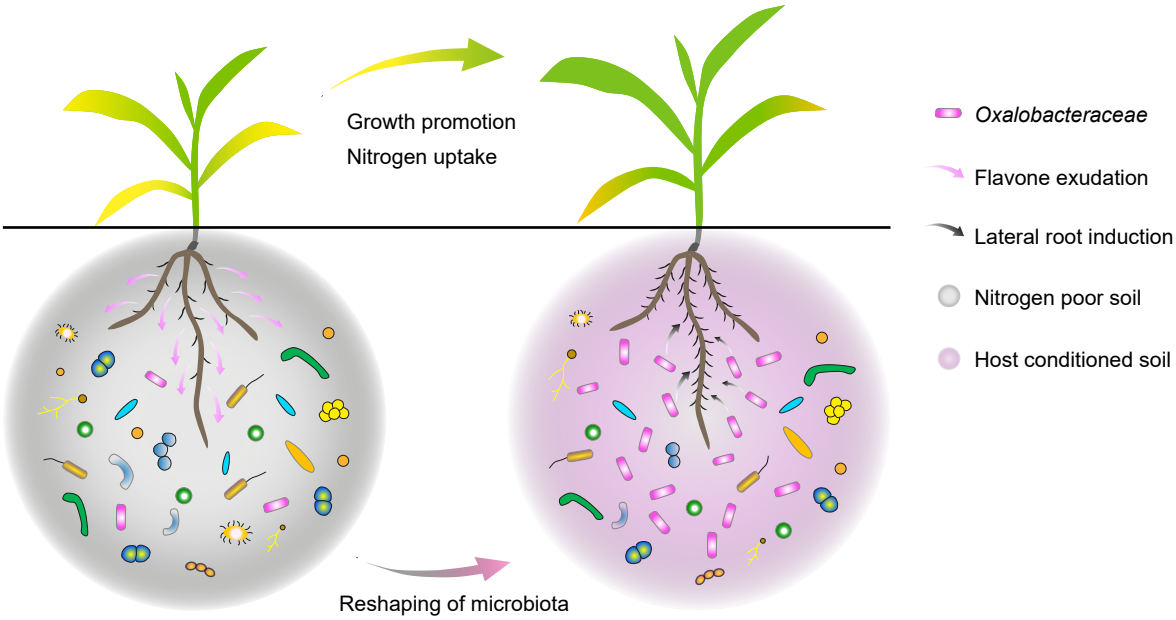
Growth promotion
Nitrogen uptake
Reshaping of microbiota
Oxalobacteraceae
Flavone exudation
Lateral root induction
Nitrogen poor soil
Host conditioned soil

Figure 6

Supplementary Figures and Tables

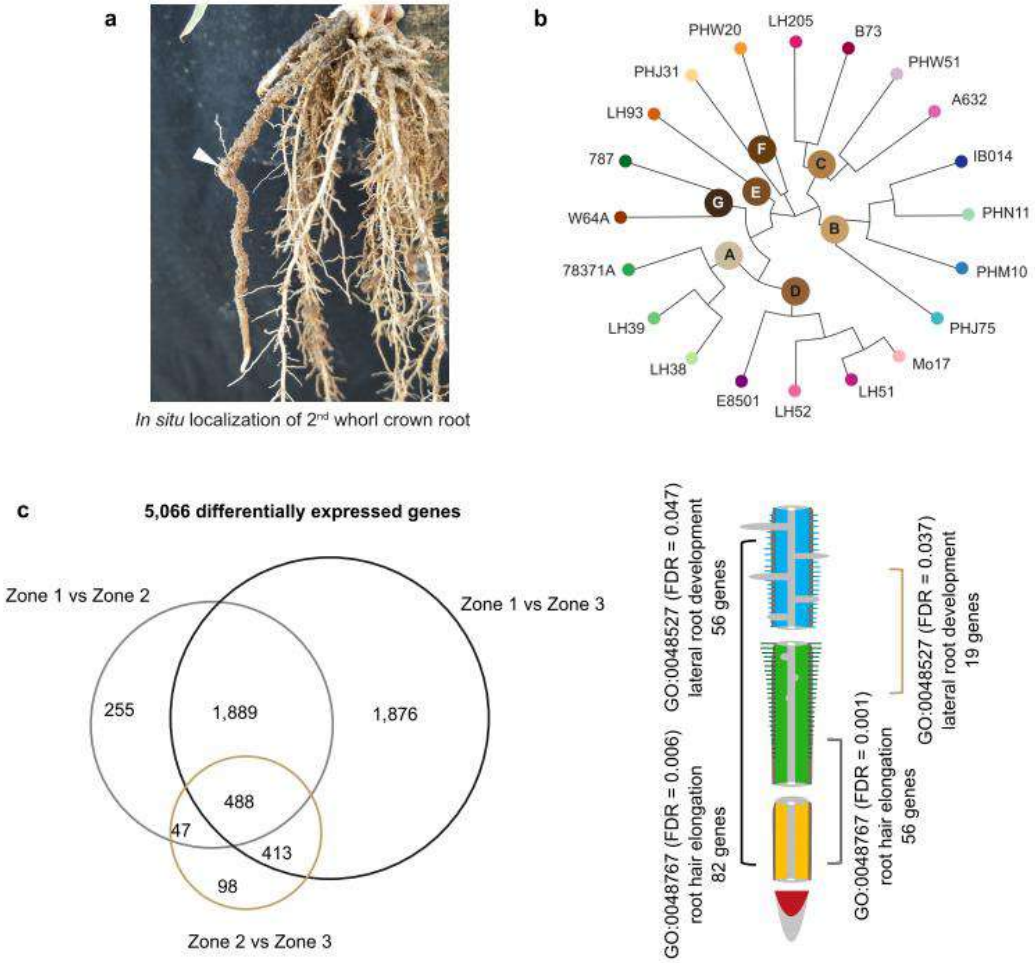

Supplementary Figure 1. Transcriptome signature synchronizes with developmental changes along the root zones of maize genotypes. a, Representative 4-week-old B73 root system from the field after removing the loosely attached soil particles by shaking. The localization of 2nd whorl of crown root with rhizosphere is indicated by a white arrow. **b**, Neighbour-joining phylogenetic tree showing relationships of 20 diverse maize inbred lines. This tree was produced based on Illumina MaizeSNP50 data. Lines were coloured and clustered into 7 groups (A-G) according to their phylogenetic distances. **c**, Venn diagram showing specificity of differentially expressed genes between each pair of zones. Separation strategy of developmental zones refers to the Figure 1a. Differentially expressed genes are declared as the fold change >2 or <-2 and FDR (false discovery rate) corrected *p* <0.05. Functional annotations (biological process) of the differentially expressed genes for each pair of zones are classified by agriGO (v2) using gene ontology (GO) with statistical significance calculated by Fisher´s exact test with Yekutieli adjustment (FDR corrected *p* <0.05). The whole list of differentially expressed genes is provided in the Supplementary Dataset 1.

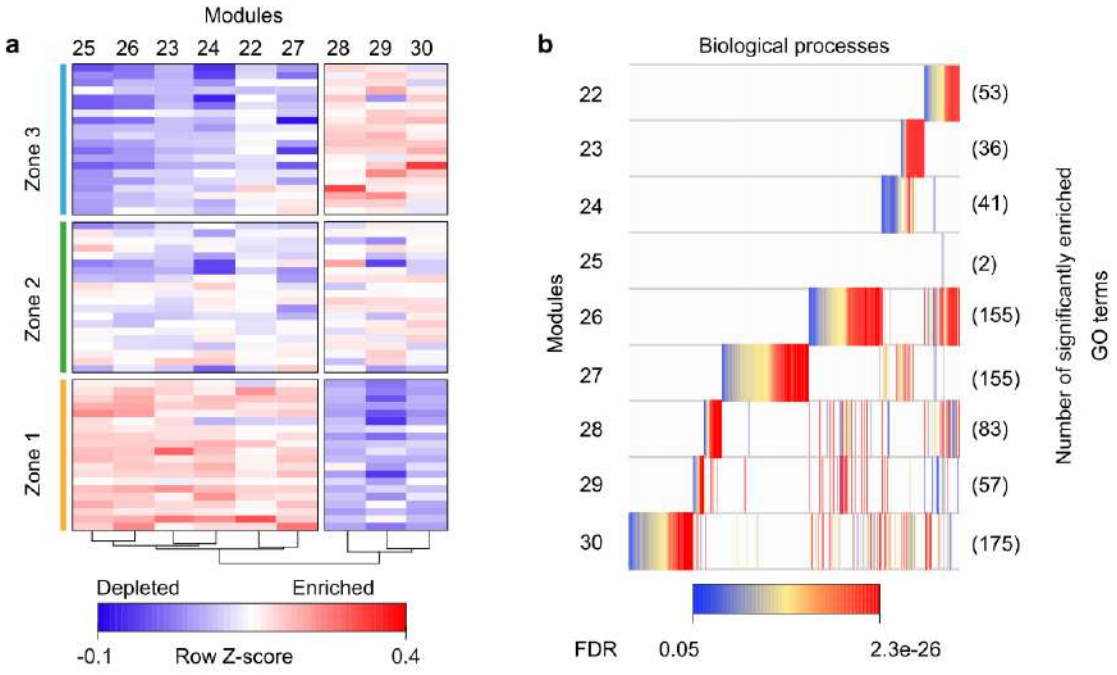

Supplementary Figure 2. Dynamic patterns and functional associations of gene co-expression modules along root developmental zones. a, Heat map illustrating six depleted and three enriched modules from the younger region to the older region along root developmental zones. **b**, Functional annotations (biological process) of genes from each module by agriGO (v2.0). The number of significant GO terms for each module is given in brackets. Statistical significance of GO enrichment for each module is calculated by Fisher´s exact test with Yekutieli adjustment (FDR corrected p <0.05).

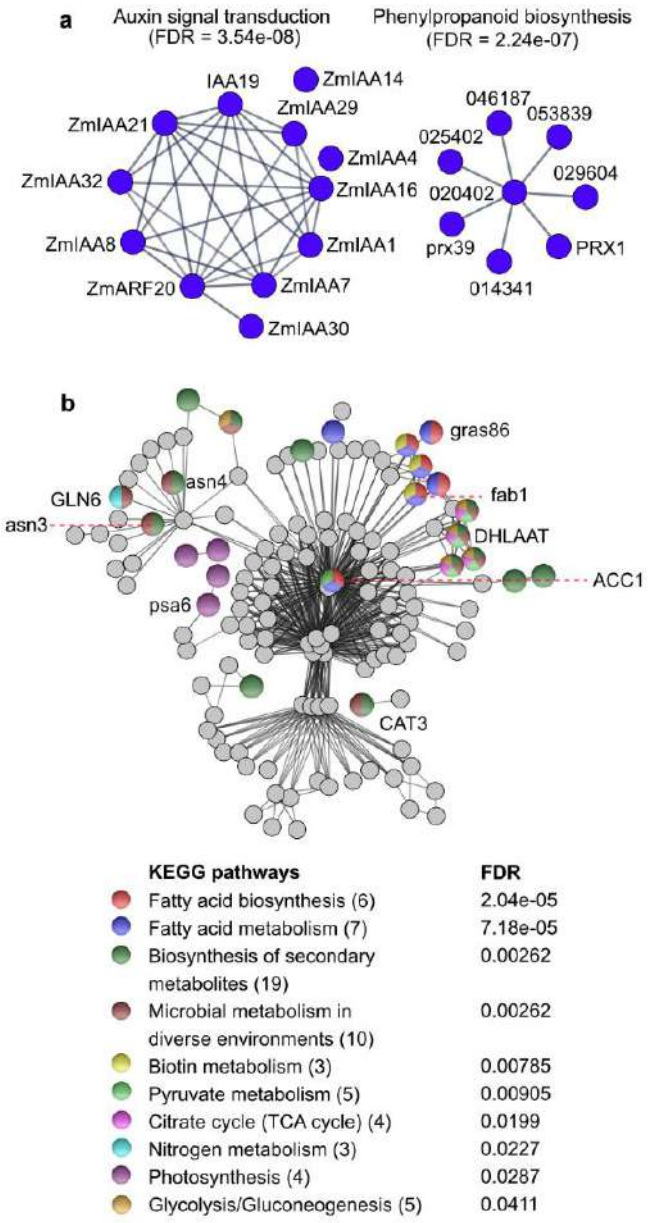

Supplementary Figure 3. Inference of protein-protein network interactions within growth (a) and defence-related (b) modules. Genes from each module were imported into the STRING database (v10.5) to query the experimentally determined interactions among genes at the high confidence 0.7 level. Those interacting genes were further functionally enriched into KEGG pathways. The significances of both networks are defined as protein-protein interaction (PPI) <1.0 e^{-16} and enriched KEGG pathways are controlled by the FDR corrected p <0.05 within the STRING database. ACC, acetyl-CoA carboxylase; ARF, auxin response factor; asn, asparagine synthetase; CAT, catalase; DHLAAT, dihydrolipoamide acetyl transferase; fab, fatty acid biosynthesis; GLN, gluthatione synthetase; IAA, indole-3-acetic acid; psa, photosystem I subunit; PRX, Peroxiredoxin. The whole list of genes enriched in networks is provided in Supplementary Datasets 5 and 6.

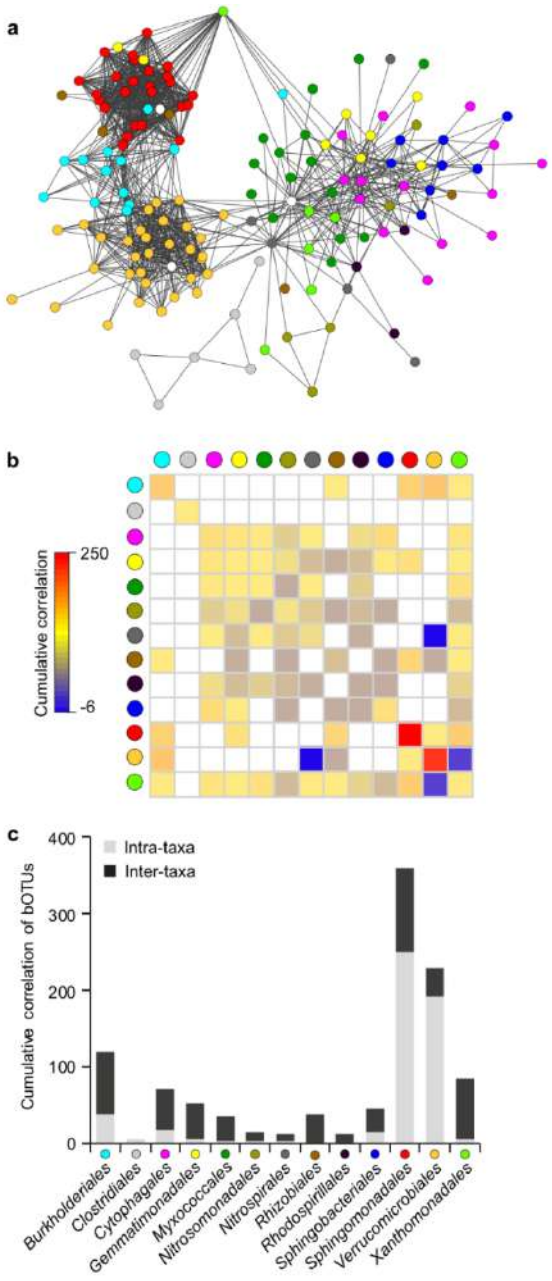

Supplementary Figure 6. Microbial network of maize rhizosphere microbiota. a, Correlation-based network of genotype and zone-associated microbial OTUs detected in the rhizosphere. Each node corresponds to an OTU, and edges between nodes correspond correlations inferred from OTU abundance profiles using the SparCC method (two-tailed pseudo *p* <0.05, correlation values <-0.6 or >0.6). The analysis was conducted with default parameters and 100 bootstrap samples were used to infer pseudo *p* values. OTUs belonging to different bacterial taxa have distinct colour codes in the rhizosphere. **b**, Cumulative correlation scores measured in the bacterial network among different bacterial orders. **c**, The proportion of edges showing inter-taxa (black) and intra-taxa (grey) correlations in the bacterial rhizosphere network.

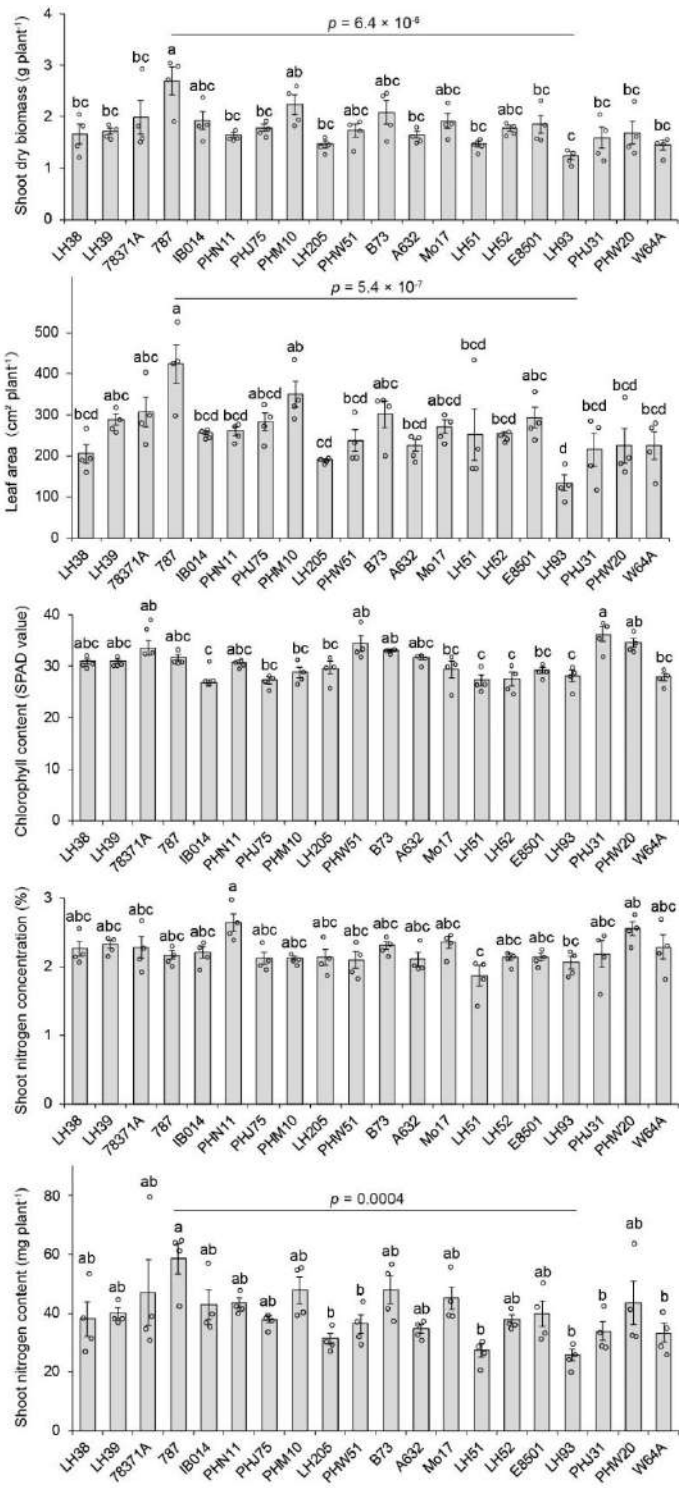

Supplementary Figure 7. Phenotypic differences of 20 maize inbred lines grown in the field. Non-destructive measurement of chlorophyll content is evaluated by SPAD (Soil Plant Analysis Development) value determined as average of 30 measurements in the middle third of the last expanded leaf. Different letters denote significance at p <0.05 (ANOVA, Tukey HSD). Significant differences between 787 and LH93 were indicated by exact p values. n = 4 biologically independent samples. Data are mean ± s.e.m.

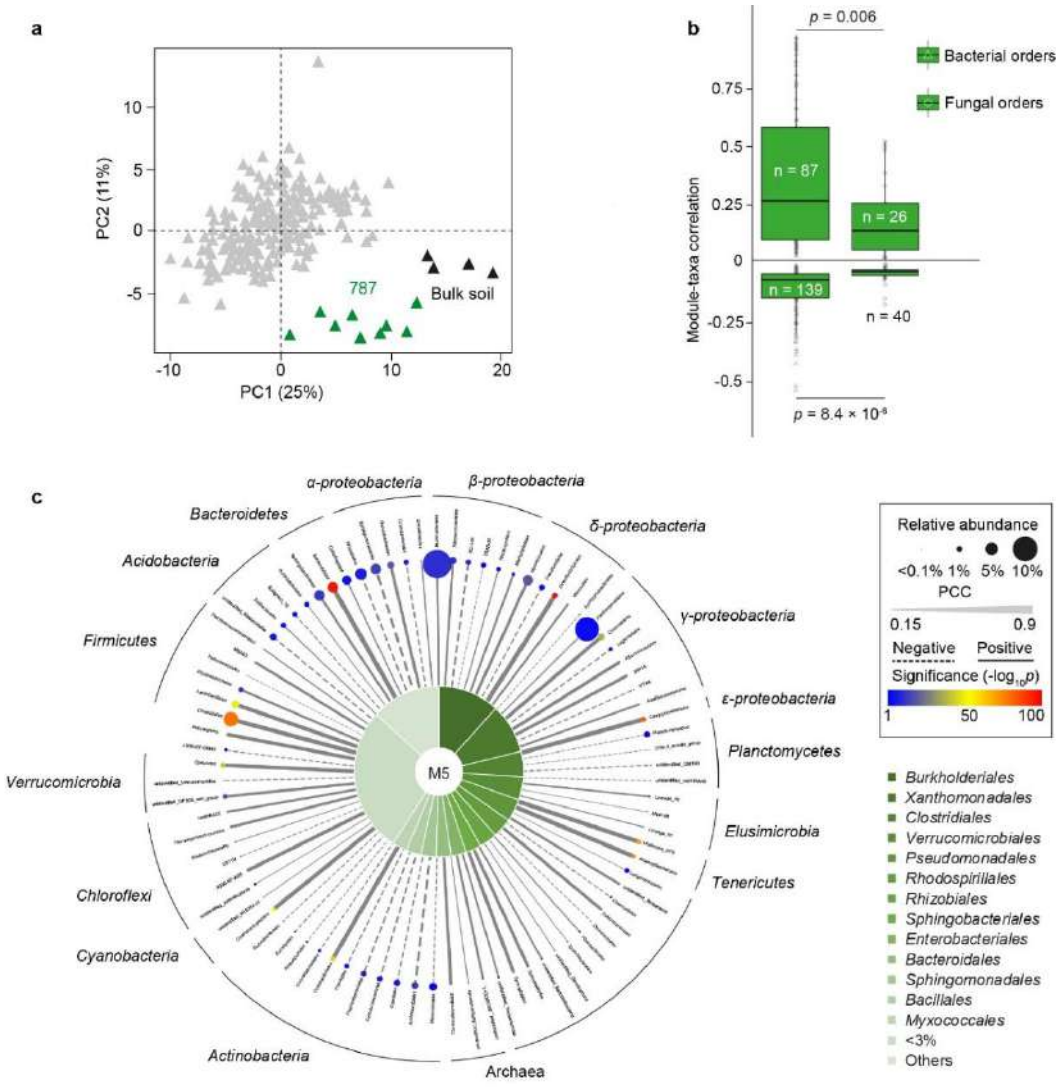

Supplementary Figure 8. Specificity of maize genotype 787 rhizosphere microbiota. a, PCA plot showing the dissimilarity of bacterial community of the 787 rhizosphere (green triangles) in comparison to the other 19 genotypes (grey triangles) and bulk soil (black triangles). **b**, Functional associations between 787-enriched module and microbial orders. *p* values, which were calculated using two-tailed Wilcoxon rank sum test, are indicating significance. The boxes span from the first to the third quartiles, the centre lines represent the median values and the whiskers show the data that lie within the 1.5 interquartile range of the lower and upper quartiles. The data points at the ends of the whiskers represent the outliers. **c**, Composition of the 787 bacterial community and its module correlation with different bacterial orders. Node size indicates the relative abundance. Edge thickness indicates the strength of Pearson's correlation coefficient. Colour scale indicates the significant levels of correlation. The exact FDR-corrected significant *p* values are shown in the Source Data.

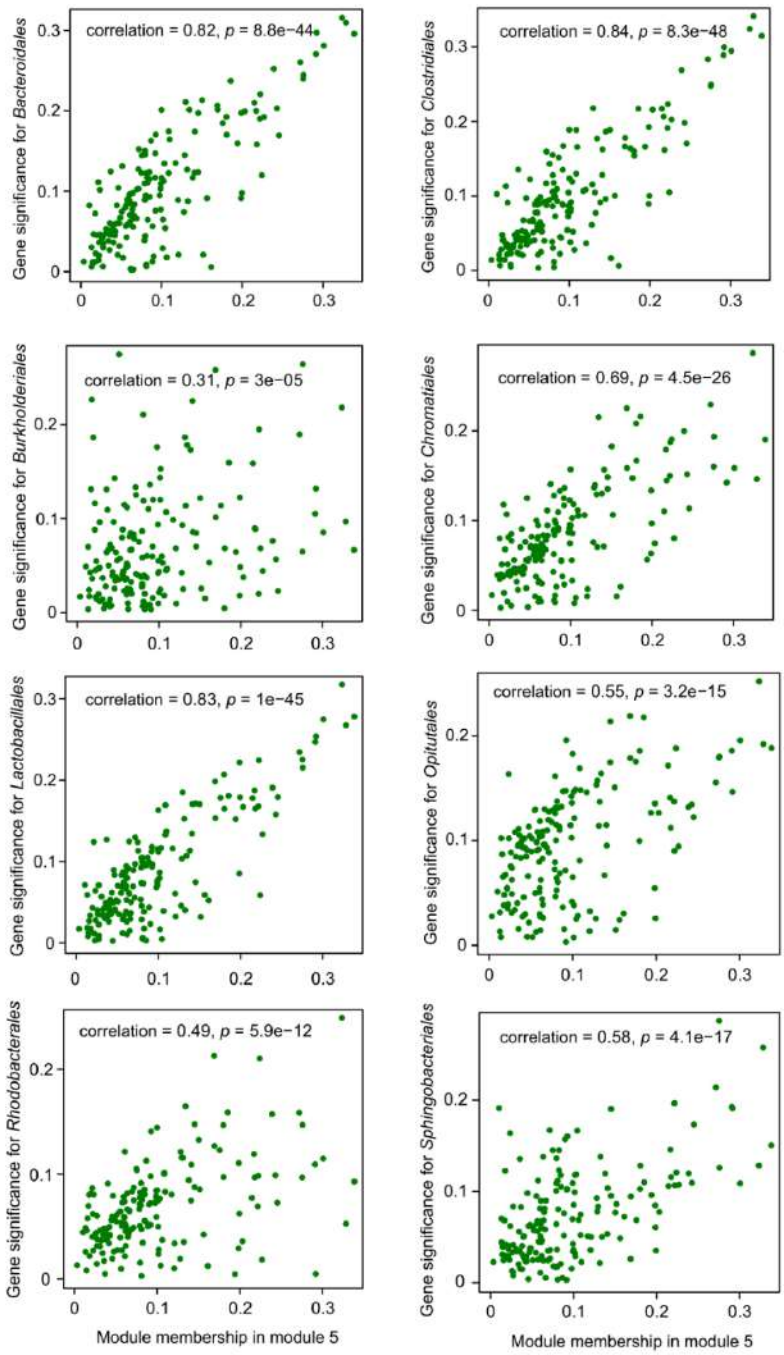

Supplementary Figure 9. Scatterplots of correlations between gene significance and module membership for 787-enriched module 5 related to specific bacterial orders. Correlation-based analysis inferred by WGCNA between 787-specific module and the bacterial taxa at the order level. Pearson's correlation is calculated by relating the eigengene of each module with the relative abundance of each taxon using WGCNA "trait" function. Gene significances between module membership are controlled by FDR corrected *p* values.

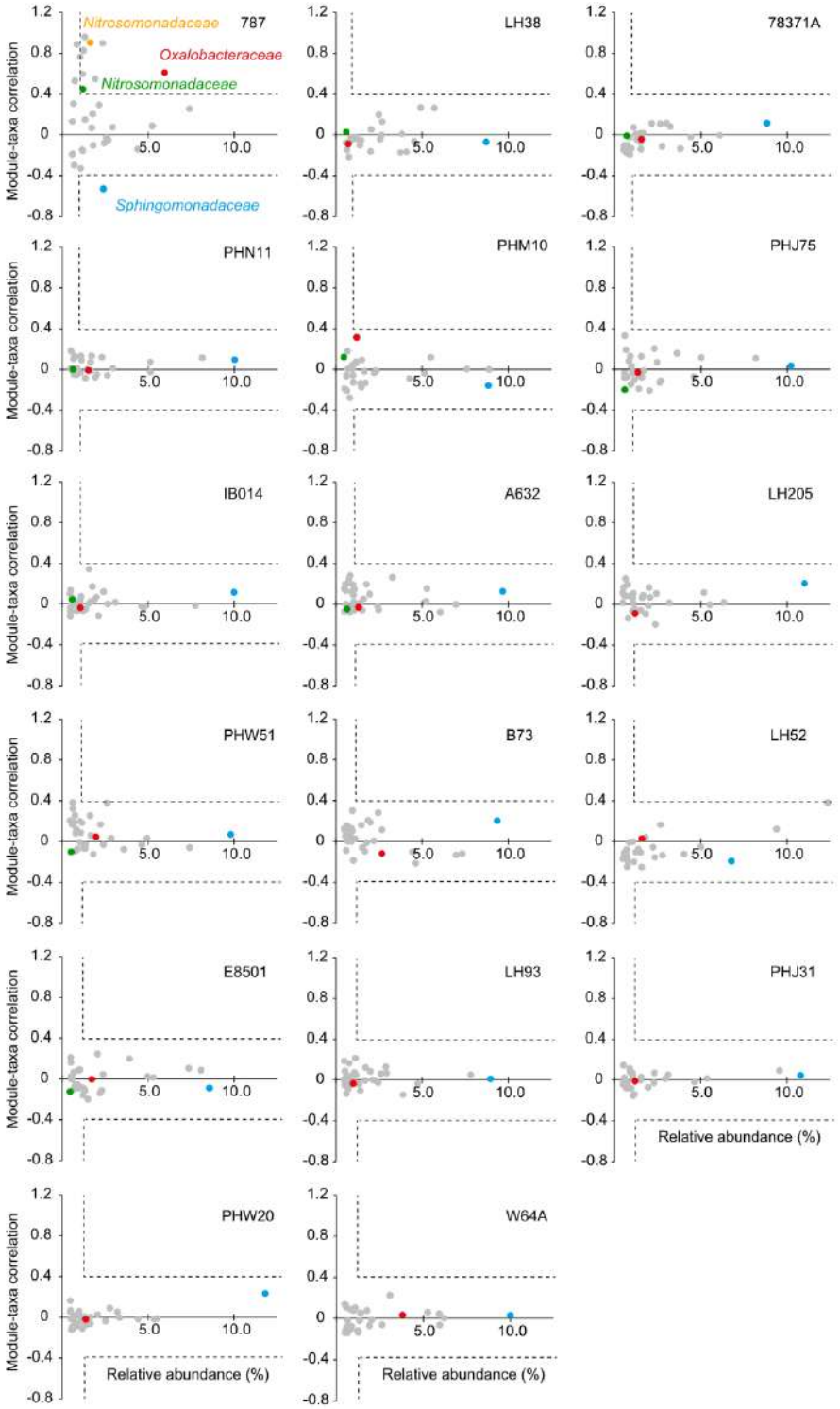

Supplementary Figure 10. Family-level module-taxa correlation highlights unique feature of 787 interaction with bacteria. These scatter plots show the Pearson's correlations between bacterial families with ≥1% relative abundance and eigengenes of genotype-specific modules (Figure 2a) identified by WGCNA. *Oxalobacteraceae* and *Sphingomonadaceae* are highlighted in red and blue for all maize inbred lines, respectively.

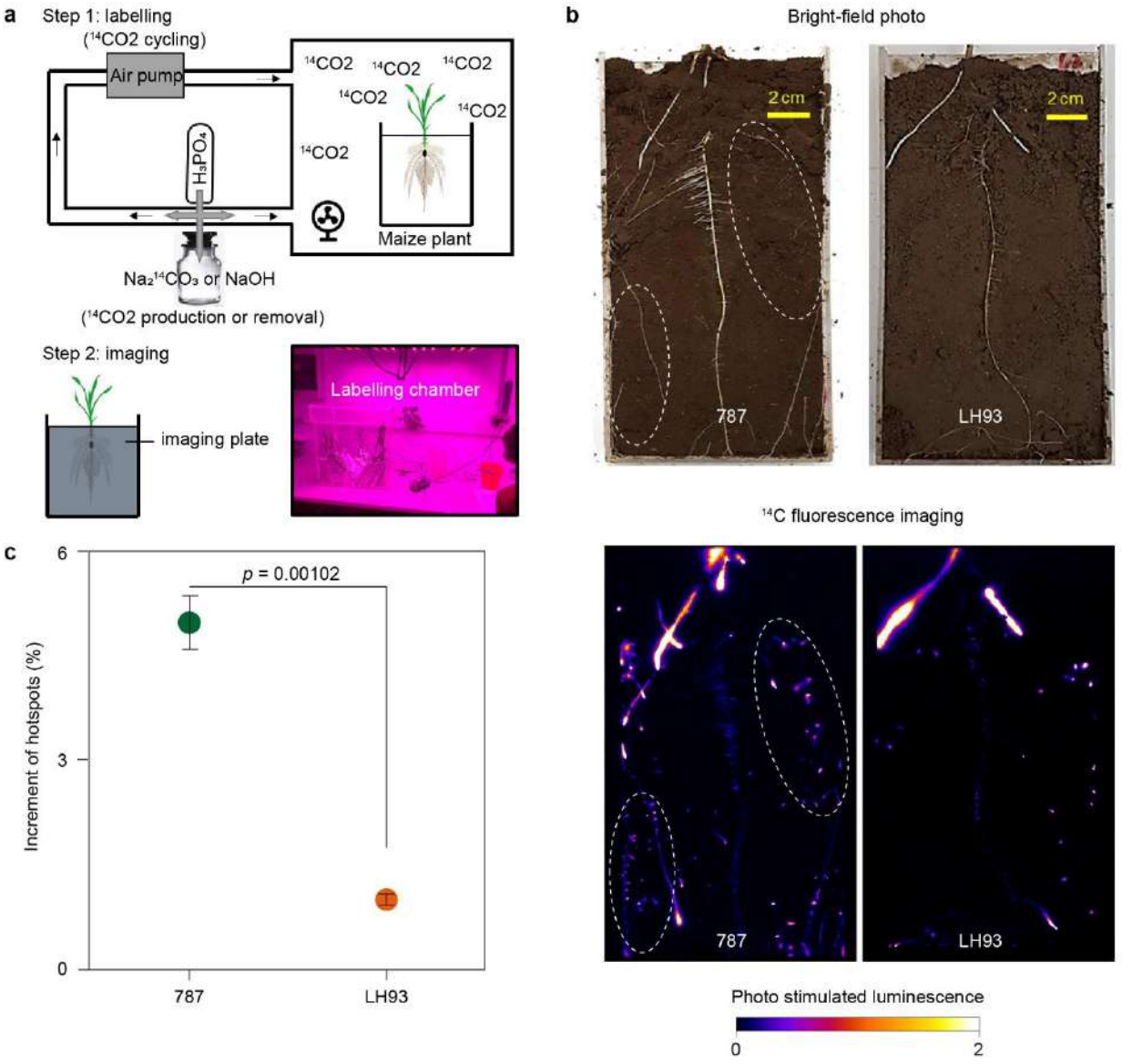

Supplementary Figure 12. Distribution of root exudates in the rhizosphere among root types between the 787 and LH93. a, Schematic illustration of ^{14}C pulse labelling and imaging for maize roots grown in the rhizobox**. b**, Comparison of root carbon exudation between 787 and LH93 by ^{14}C pulse labelling and imaging. Hot spots of exudation from the lateral roots are highlighted by the dotted circles. **c**, Quantification results are shown as increment of the hotspots (%). Data are presented as mean values ± s.e.m and *n* = 3 biologically independent samples. Significance was calculated using two-tailed unpaired t-test and indicated with exact value.

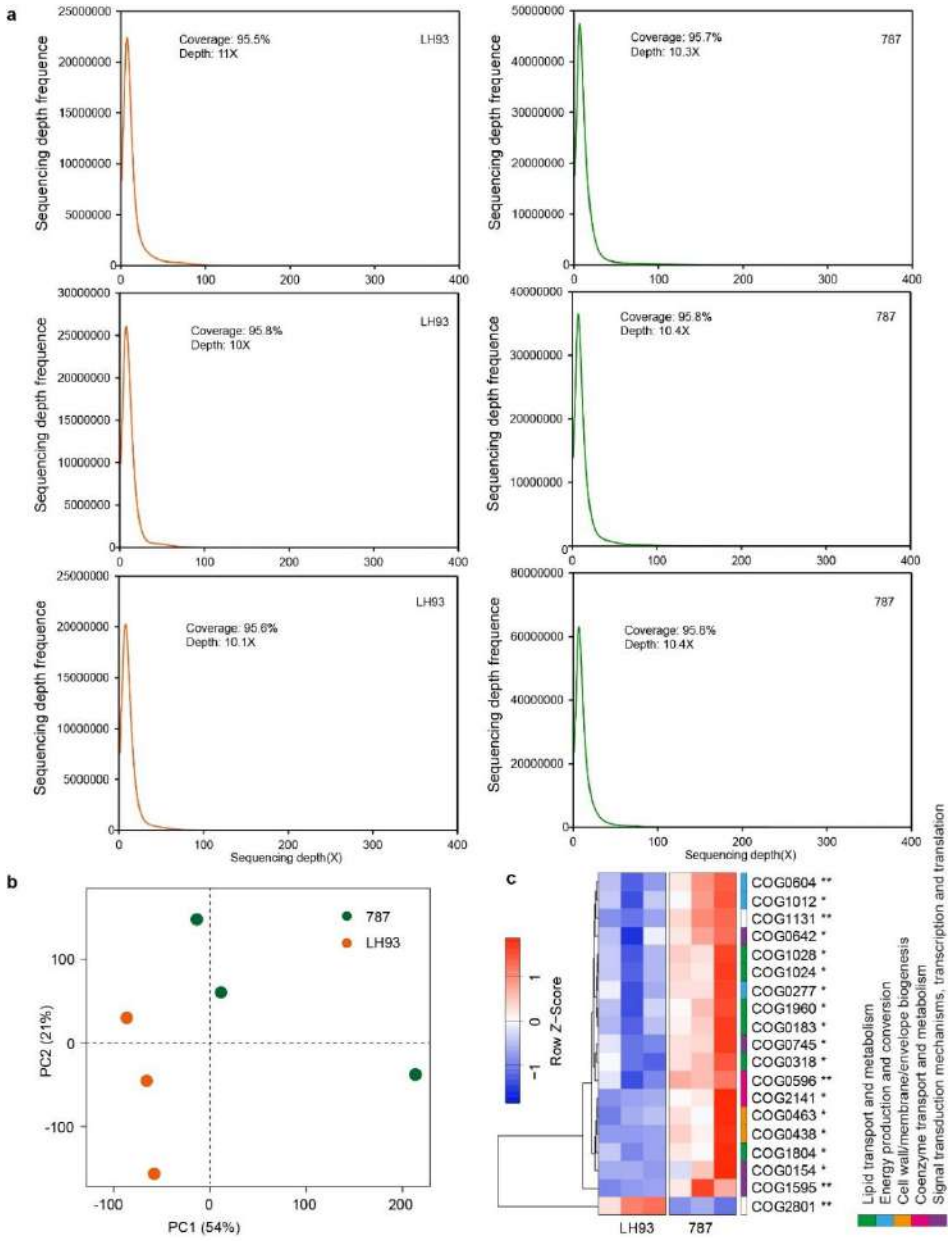

Supplementary Figure 14. Functional differences between the 787 and LH93 microbiomes. a, Coverage and sequencing depth of shotgun metagenomics sequencing of 787 and LH93 rhizosphere microbiomes. **b**, PCA plot indicating distinct functional gene profiles associated with 787 and LH93 rhizosphere metagenome. **c**, Enrichment of functional categories of COG (Clusters of Orthologous Groups) families for the rhizosphere metagenome between 787 and LH93. Mean proportion of functional genes (%) normalized by Row-Z score and asterisks indicate significant differences between 787 and LH93 rhizosphere microbiome with two-tailed unpaired t-test (FDR adjusted *p <0.05, **p <0.01). n = 3 biologically independent samples.

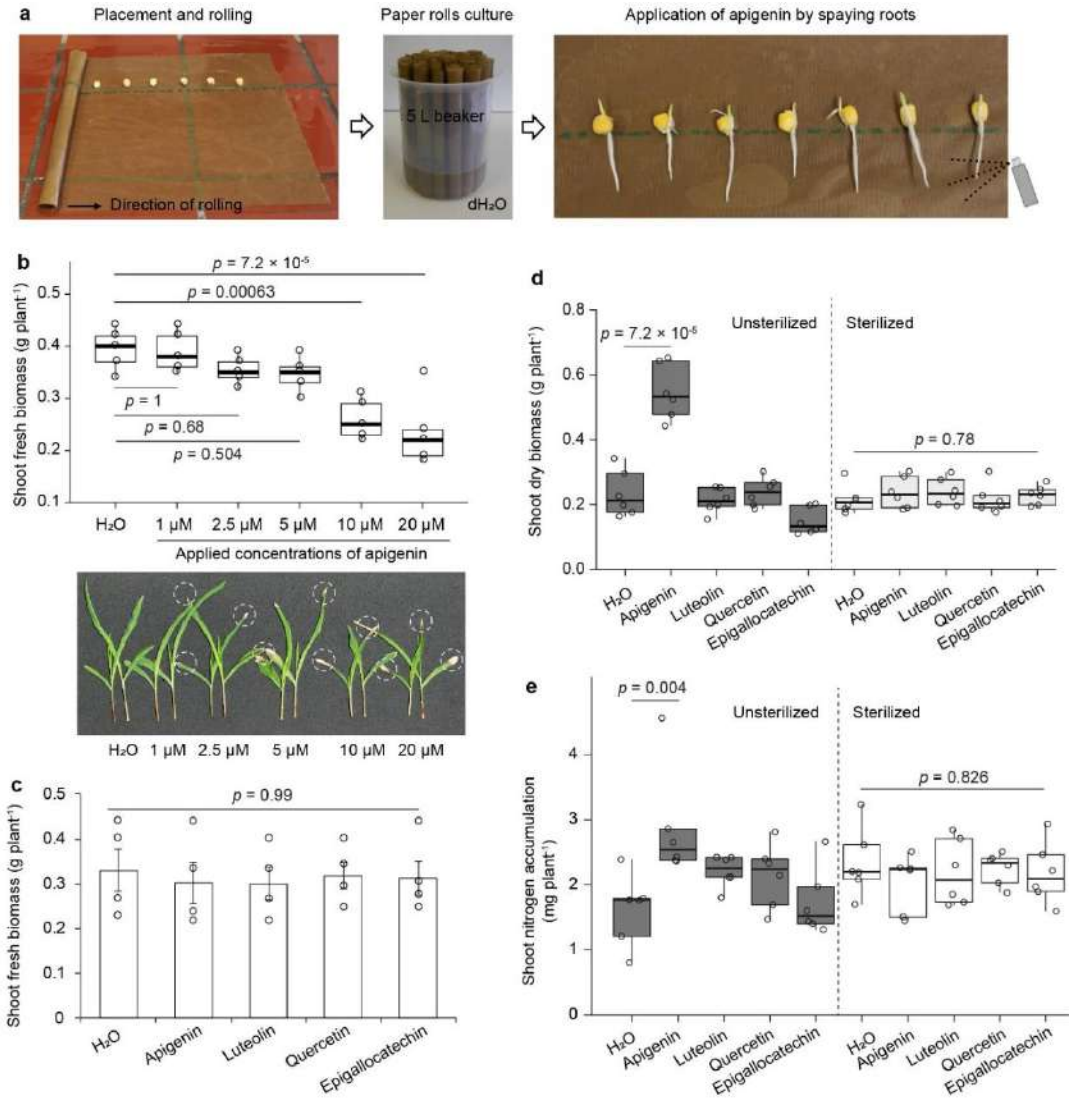

Supplementary Figure 15. Effects of exogenous flavonoids on maize growth in the paper roll system and soil pots. a, Illustration of the paper roll system used in this study and workflow for flavonoid application. **b**, Effects of different concentrations of apigenin on maize shoot growth in the paper roll system. *n* = 5 biologically independent samples. The top and bottom of boxes indicate interquartile range (75% to 25% of the data) and the median values are shown as horizontal bars within boxes. Leaf damages caused by over-applied concentrations of apigenin are highlighted by dotted circles. **c**, Effects of different types of flavonoids (1 μM) on maize shoot growth in the paper roll system. *n* = 4 biologically independent samples. Data are mean ± s.e.m. Effects of exogenously applied flavonoid types on *C2-idf* growth (**d**) and nitrogen accumulation (**e**) in nitrogen-poor soil with and without prior sterilization. For **d** and **e**, *n* = 6 biologically independent samples. For **b**, **d** and **e**, the boxes span from the first to the third quartiles, the centre lines represent the median values and the whiskers show the data that lie within the 1.5 interquartile range of the lower and upper quartiles. The data points at the ends of the whiskers represent the outliers. For **b**, **c**, **d** and **e**, significances were indicated among different groups by exact *p* values (ANOVA, Tukey HSD).

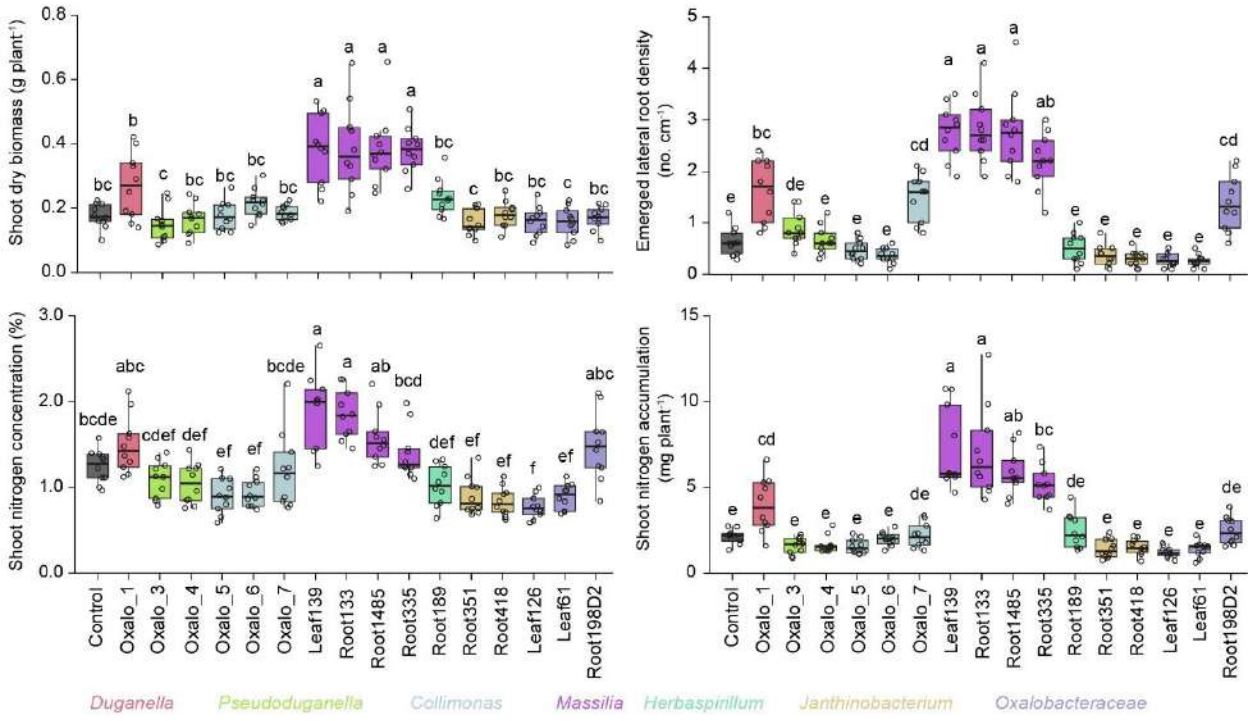

Supplementary Figure 18. Effects of *Oxalobacteraceae* strains inoculation on growth promotion and nitrogen uptake in *Irt1* mutant in nitrogen-poor soil. Different letters indicate significantly different groups (p <0.05, ANOVA, Tukey HSD). n = 10 biologically independent samples over two independent inoculation experiments. The boxes span from the first to the third quartiles, the centre lines represent the median values and the whiskers show the data that lie within the 1.5 interquartile range of the lower and upper quartiles. The data points at the ends of the whiskers represent the outliers.

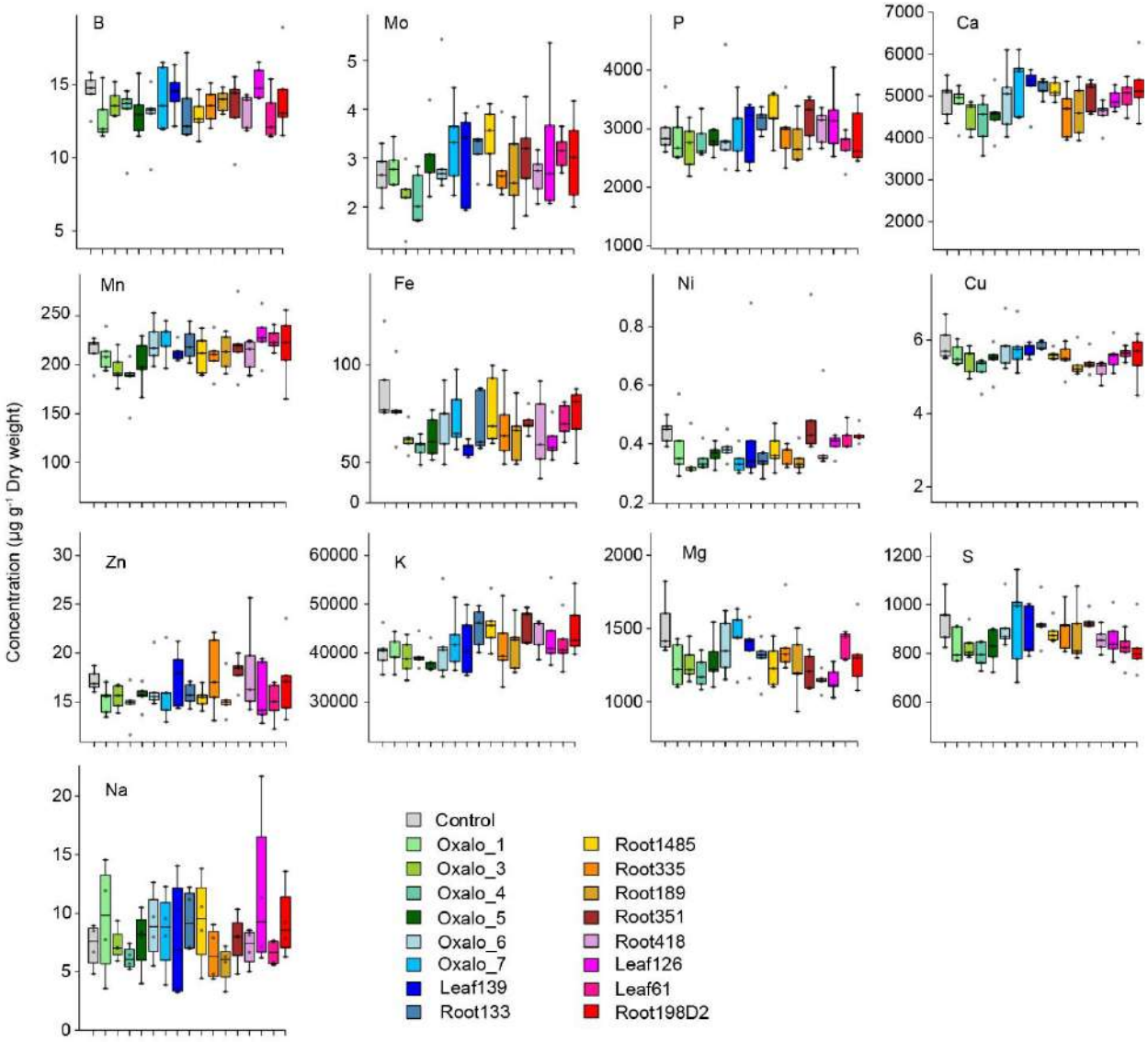

Supplementary Figure 19. Effects of *Oxalobacteraceae* strains inoculation on the concentrations of 13 mineral nutrients in *Irt1* mutant in nitrogen-poor soil. No significant differences were detected at $p < 0.05$ (ANOVA, Tukey HSD). $n = 5$ biologically independent samples. The boxes span from the first to the third quartiles, the centre lines represent the median values and the whiskers show the data that lie within the 1.5 interquartile range of the lower and upper quartiles. The data points at the ends of the whiskers represent the outliers.

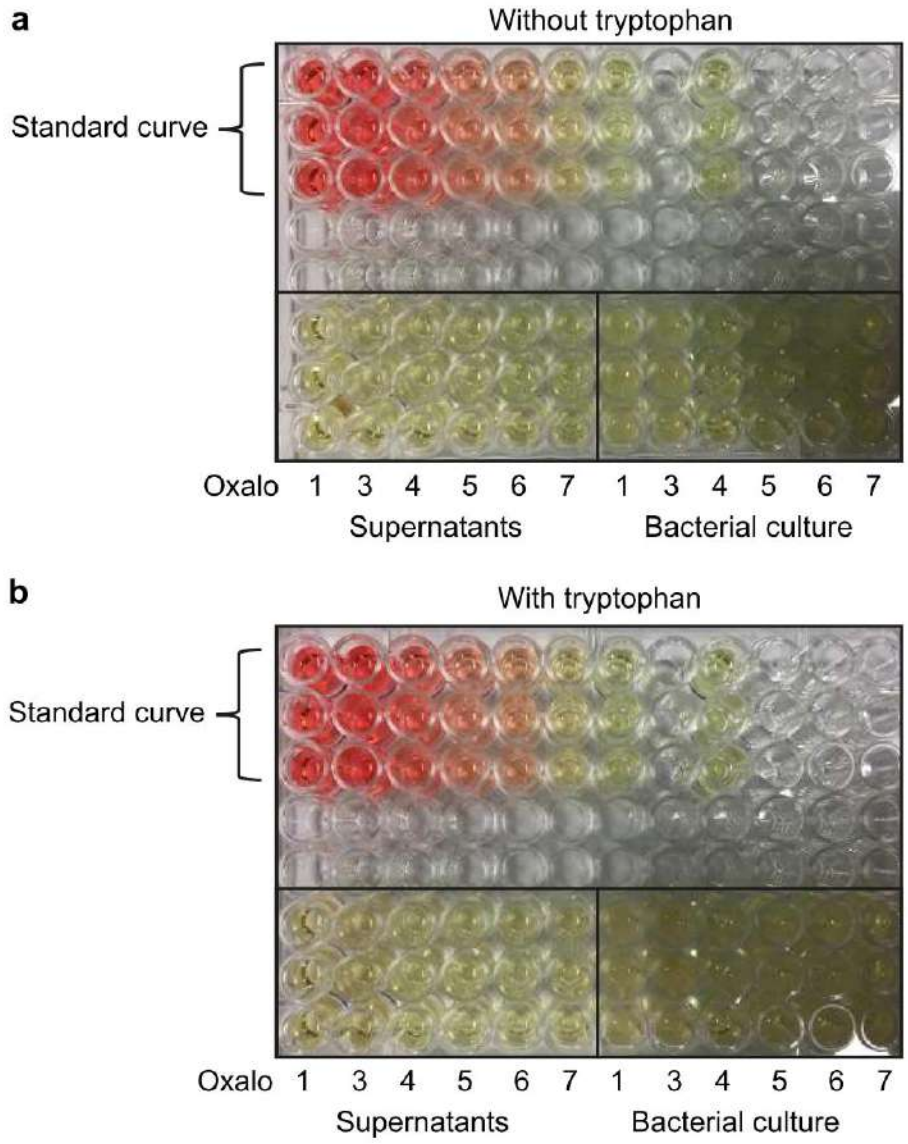

Supplementary Figure 21. Determination of indolic compounds produced by *Oxalobacteraceae* strains based on supernatants and bacterial cultures. a, Without tryptophan. **b**, With tryptophan. Colorimetric analysis by the reagent of Salkowski of stationary phase cultures indicated that *Oxalobacteraceae* isolates do not produce auxin in the presence and absence of tryptophan.

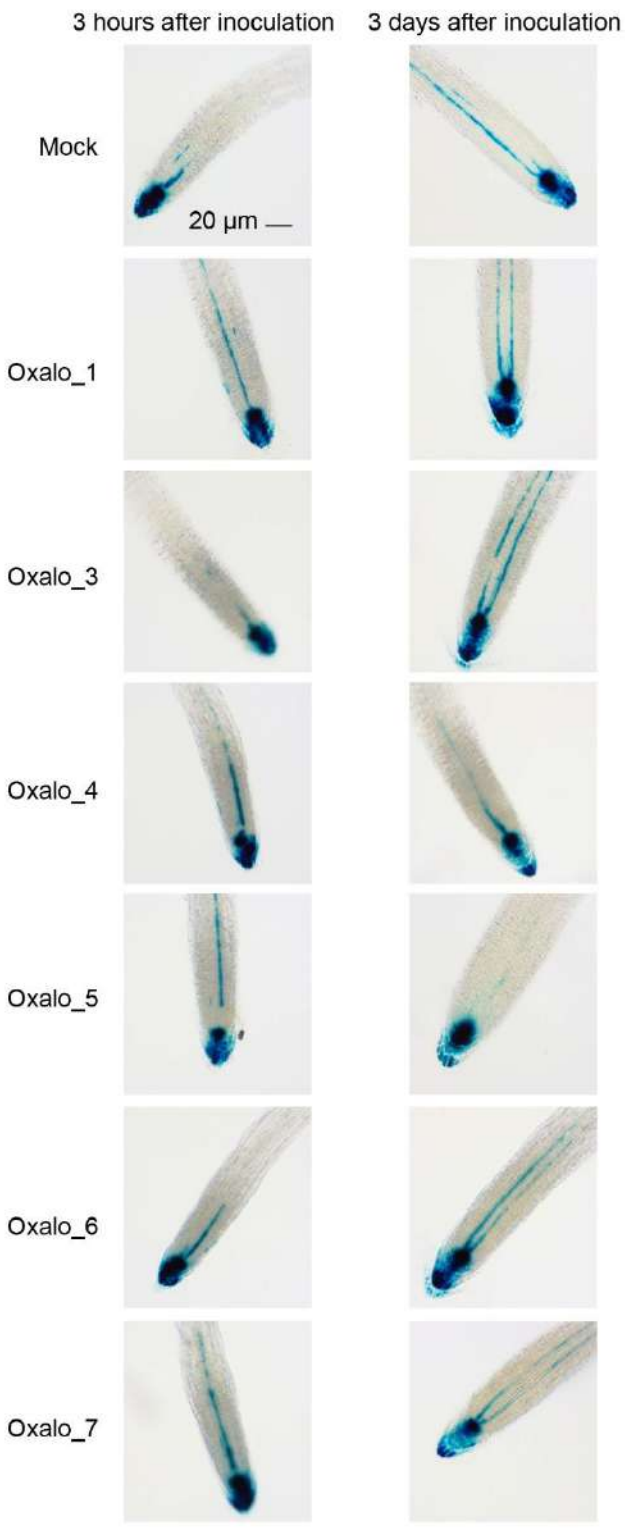

Supplementary Figure 22. Auxin induction tests in Arabidopsis by *Oxalobacteraceae* strains. Expression of *DR5::GUS* signal along the longitudinal root of *Arabidopsis* after 3 h and 3 d inoculation with different *Oxalobacteraceae* strains.

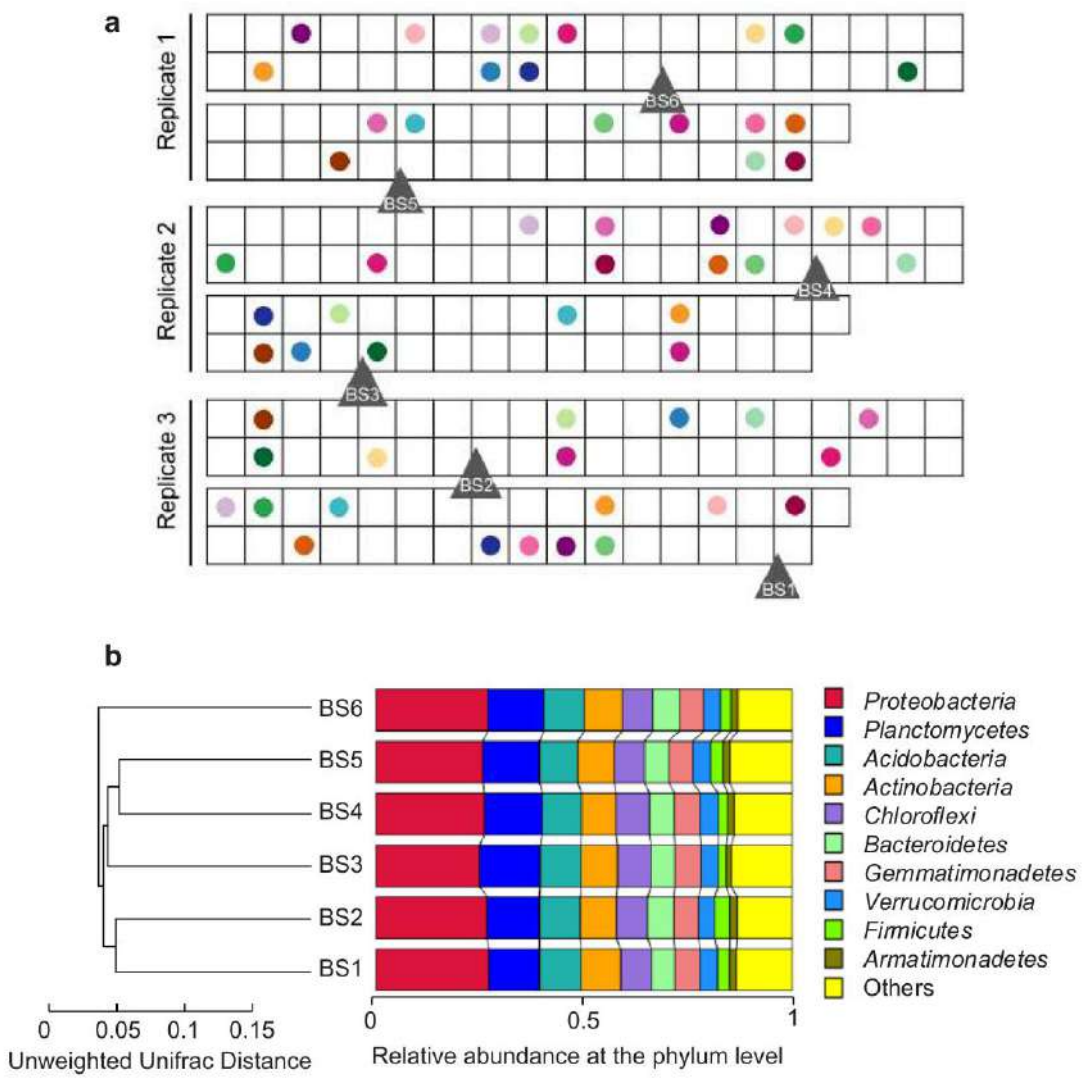

Supplementary Figure 23. The experimental design, germplasm used and soil homogeneity in this field study. a, Complete random design of the field experiment and sampling sites of the maize inbred lines. In total, 72 US public inbred lines from the Ames population were sown in the field and the coloured 20 healthy grown lines indicate their distributions for three biological replicates in the field. Six basic soil samples with the triangle symbols were collected for preliminary test of bacterial diversity before sowing. Colour dots correspond to different maize genotypes in Supplementary Fig. 1b. **b**, Homogeneous distribution of bulk soil microbiome from the basic soil samples. β-diversity heat map was compared for six basic soil samples at the phylum level using unweighted unifrac distance. BS, basic soil.

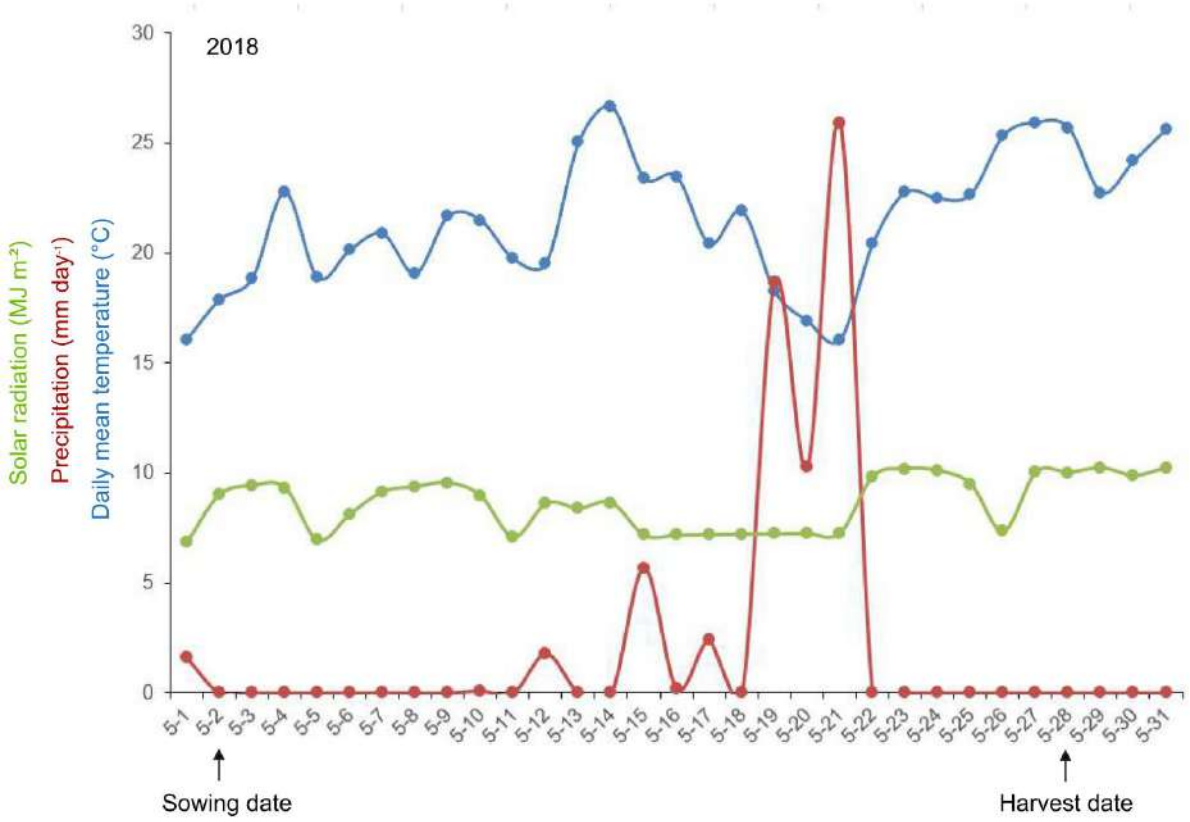

Supplementary Figure 24. Meteorological data tracked during the 4-week growth period in the field. Daily mean temperature, precipitation per day and solar radiation were colour-coded accordingly. The sowing and harvest dates were indicated by black arrows.

Supplementary Table 3. Interactions of the gene and OTU according to significant factors. The pre-filtered genes were used as input to identify differentially expressed genes for each OTU (bacterial and fungal) by using the R package DESeq2 with the model gene expression ~ OTU abundance. OTU abundance was taken as a trait to explain gene expression. Significant genes were determined with corresponding bOTUs and fOTUs with FDR and log_2 fold change for α levels of 0.001. The same analysis was performed as above but explaining bOTU abundance with fOTU abundance and vice versa.

	x	**Total x**	**Unique x**	**% unique**	**y**	**Total y**	**sign. y>0 x**	**% sign. y**	**Total x**	**x per y**
Genes~bOTU-1%	**Genes**	27092	12907	0.48	**bOTU**	736	720	0.98	797361	1107
Genes~bOTU-0.1%	**Genes**	27092	7342	0.27	**bOTU**	736	700	0.95	284729	407
Genes~fOTU-1%	**Genes**	27092	4043	0.15	**fOTU**	18	18	1	8248	458
Genes~fOTU-0.1%	**Genes**	27092	1553	0.06	**fOTU**	18	17	0.94	2761	162
bOTU~fOTU-1%	**bOTU**	736	47	0.06	**fOTU**	18	11	0.61	75	7
bOTU~fOTU-0.1%	**bOTU**	736	12	0.02	**fOTU**	18	9	0.5	16	2
fOTU~bOTU-1%	**fOTU**	18	1	0.06	**bOTU**	736	3	0	3	1
fOTU~bOTU-0.1%	**fOTU**	18	0	0	**bOTU**	736	0	0	0	0

Overlap	**Genes_OTUs**	**Total x**	**Overlap**	**% of total**	**Unique**	**% of total**
Genes~bOTU-1%	12907	13402	3549	0.26	9359	0.7
Genes~fOTU-1%	4043	13402	3549	0.26	494	0.04
Genes~bOTU-0.1%	7342	7534	1363	0.18	5980	0.79
Genes~fOTU-0.1%	1553	7534	1363	0.18	191	0.03

Supplementary Table 4. Basic soil chemical properties before fertilization in the field.

Parameters	pH	Organic matter content (g/kg)	Total nitrogen (g/kg)	Available phosphorus (mg/kg)	Exchangeable potassium (mg/kg)
Values	8.5	14.1	0.9	6.7	100.4